

THESIS

OBSERVATIONS AND SIMULATIONS OF THE INTERACTIONS BETWEEN  
CLOUDS, RADIATION, AND PRECIPITATION

Submitted by

Alexandra Claire Naegele

Department of Atmospheric Science

In partial fulfillment of the requirements

For the Degree of Master of Science

Colorado State University

Fort Collins, Colorado

Fall 2016

Master's Committee:

Advisor: David A. Randall

Christian D. Kummerow

Jorge A. Ramirez

Copyright by Alexandra Claire Naegele 2016

All Rights Reserved

## ABSTRACT

# OBSERVATIONS AND SIMULATIONS OF THE INTERACTIONS BETWEEN CLOUDS, RADIATION, AND PRECIPITATION

The first part of this study focuses on the radiative constraint on the hydrologic cycle as seen in observations. In the global energy budget, the atmospheric radiative cooling (ARC) is approximately balanced by latent heating, but on regional scales, the ARC and precipitation are inversely related. We use precipitation data from the Global Precipitation Climatology Project and radiative flux data from the Clouds and the Earth's Radiant Energy System (CERES) project to investigate the radiative constraint on the hydrologic cycle and how it changes in both space and time. We find that the effect of clouds is to decrease the ARC in the tropics, and to increase the ARC in middle and higher latitudes. We find that, spatially, precipitation and the ARC are negatively correlated in the tropics, and positively correlated in middle and higher latitudes. In terms of the global mean, the precipitation rate and the ARC are temporally out-of-phase during the Northern Hemisphere winter.

In the second part of this study, we use a cloud-resolving model to gain a deeper understanding of the relationship between precipitation and the ARC. In particular, we explore how the relationship between precipitation and the ARC is affected by convective aggregation, in which the convective activity is confined to a small portion of the domain that is surrounded by a much larger region of dry, subsiding air. We investigate the responses of the ARC and precipitation rate to changes in the sea surface temperature (SST), domain size, and microphysics parameterization. Both fields increase with increasing SST and the use of 2-moment microphysics. The precipitation and ARC show evidence of convective aggregation, and in the domain average, both fields increase as a result.

While running these sensitivity tests, we observed a pulsation in the convective precipitation rate, once aggregation had occurred. The period of the pulsation is on the order of ten simulated hours for a domain size of 768 km. The sensitivity tests mentioned above were used to investigate the mechanism of the pulsation. We also performed an additional test with no evaporation of falling rain, which leads to no cold pools in the boundary layer. Our results show that the period of the pulsation is noticeably sensitive to microphysics and domain size. The pulsation disappears completely when cold pools are prevented from forming, which suggests a “discharge-recharge” mechanism.

## ACKNOWLEDGEMENTS

I thank my advisor, Dr. David Randall for sharing his ideas with me and for listening to my own. His passion for his work is an inspiration. Thank you to Dr. Chris Kummerow and Dr. Jorge Ramirez for serving on my committee. A special thanks to Don Dazlich for his patience and time teaching me to use SAM. Thank you to the Randall group and CMMAP neighbors for feedback, insight, and helpful discussions. And thank you to my family and friends, both near and far, for all the support and encouragement along the way.

This thesis is typeset in  $\text{\LaTeX}$  using a document class designed by Leif Anderson.

## TABLE OF CONTENTS

Abstract .....	ii
Acknowledgements .....	iv
List of Tables .....	viii
List of Figures .....	ix
Chapter 1. Energetic Constraints on the Hydrologic Cycle .....	1
Chapter 2. Data and Methods .....	8
2.1. Data.....	8
2.2. Methods.....	9
Chapter 3. Observed Radiative Constraints on the Hydrologic Cycle.....	10
3.1. Climatology.....	10
3.2. Effects of Clouds.....	13
3.3. Seasonal Correlations .....	16
3.4. Conclusions.....	21
Chapter 4. Bridge .....	22
Chapter 5. Summary of Previous Work on Aggregated Convection .....	28
5.1. Hysteresis.....	29
5.2. Sensitivities.....	30
5.3. Possible Mechanisms.....	33
5.4. Role of Radiative and Surface Fluxes.....	34

5.5. Observational Evidence .....	36
Chapter 6. Model Setup .....	38
6.1. System for Atmospheric Modeling.....	38
6.2. Sensitivity Tests .....	39
6.3. Quantifying Aggregation Strength.....	40
Chapter 7. Effects of Convective Aggregation on the Radiative Constraint on Precipitation in the SAM.....	41
7.1. Quantifying Aggregation Strength.....	41
7.2. Time-series Analyses: Effects of Convective Aggregation.....	44
7.3. Sensitivity Testing .....	53
7.4. Temporal Correlation Between Precipitation and ARC .....	55
7.5. Effect of Clouds on the ARC.....	62
7.6. Conclusions.....	63
Chapter 8. Pulsation of Aggregated Convection in SAM.....	65
8.1. Overview of the Phenomenon .....	65
8.2. Hypotheses .....	65
8.3. Sensitivity Testing .....	66
8.4. Conclusions.....	73
Chapter 9. Discussion and Conclusions.....	74
9.1. Observations.....	74
9.2. Bridge.....	76
9.3. Effects of Convective Aggregation on the Atmospheric Energy Balance and Hydrologic Cycle in SAM.....	76

9.4. Pulsating Aggregated Convection .....	79
9.5. Implications for Future Work .....	80
References .....	82



## LIST OF TABLES

7.1	Overview of the simulations and the name used for reference. ....	44
-----	---	----

## LIST OF FIGURES

1.1	The rate at which precipitation increases (according to 10 GCM in CMIP3) differs greatly from that expected with the Clausius-Clapeyron approximation. From Allen and Ingram (2002).....	2
1.2	CMIP3 models show a strong positive relationship between the changes in latent heating ad radiative cooling. From Stephens and Ellis, 2008.....	7
3.1	Precipitation climatology from GPCP monthly means (1979 - 2014).....	11
3.2	(a) all-sky ARC, (b) clear-sky ARC, (c) all-sky - clear-sky ARC. Climatology from CERES monthly means (2001 - 2014).....	12
3.3	ARC and Precipitation seasonal cycle from monthly means.....	14
3.4	ARC and Precipitation interannual variability (deseasonalized).....	14
3.5	Radiative effect of clouds on the total ARC and on ARC components.....	17
3.6	Seasonal correlation between ARC and precipitation using monthly means.....	18
3.7	(a) Zonally averaged correlation of ARC and precipitation (left), (b) Correlation of zonally averaged ARC and precipitation (right).....	18
3.8	Zonally averaged standard deviants of (a) ARC (left) and (b) Precipitation (right).	19
3.9	The zonally averaged seasonal composite of (a) ARC (left) and (b) Precipitation (right).....	20
4.1	The change in the percent anomaly of the global mean SSM/I precipitation rate is shown by the black curve. From Wentz et al., 2007.....	23
4.2	Correlation between the pattern amplification of Sea Surface Salinity and the the change in SST. From Durack et al., 2012.....	24

7.1	Suite of statistics on PW distribution that are useful in identifying the evolution and onset of aggregation .....	42
7.2	Contour plot of the PDF of (a) PW (left), and (b) ARC (right), over the domain at each timestep. The color represents the ( $\log_{10}$ ) fraction of grid points within each bin. ....	43
7.3	Domain averages of the fluxes contributing to the atmospheric energy balance. (a) Precipitation (top), (b) ARC (second from top), (c) SHF (second from bottom), (d) Net (bottom).....	46
7.4	Maps of the surface precipitation rate averaged over 24 hours.....	47
7.5	Maps of PW averaged over 24 hours.....	48
7.6	Running means of the domain-averaged precipitation and ARC.....	49
7.7	Maps of ARC averaged over 24 hours.....	51
7.8	Maps of OLR averaged over 24 hours.....	52
7.9	Comparison of domain-averaged ARC and Precipitation rates at 300 and 305 K , and 480 and 768 km domain. ....	54
7.10	Comparison of (a) ARC (top), (b) Precipitation (middle), and (c) PW (bottom) with 1-moment and 2-moment microphysics. ....	55
7.11	Domain-averaged high cloud fraction. ....	56
7.12	2D representation of the temporal correlation between ARC and precipitation at each grid point with (a) no averaging (left) and (b) averaged over 30 days (right). ....	57
7.13	Running means of the domain-averaged net atmospheric energy balance. ....	59

7.14	Changes in ARC plotted against changes in atmospheric heating; running means with various window sizes have been applied. The color indicates the time in hours. ....	61
7.15	The cloud effect on the ARC in the baseline simulation. ....	63
7.16	A comparison of the cloud effects on the ARC in the baseline and 768HI-2 simulations. ....	63
8.1	Snapshot of the surface precipitation pulsing at a relative minimum (left) and maximum (right). ....	66
8.2	Top two panels are of 768HI-2 (a) over the entire simulation and (b) with a close up of the final 10 days. Bottom panels (c,d) are the same, but for 480HI-2. ....	68
8.3	Spectral analysis of (a) 480HI-2 (top left), (b) 768HI-2 (bottom left), (c) 480LO-2 (top right), (b) 768HLO-2 (bottom right) ....	69
8.4	Domain-averaged (a) precipitation (top) and (b) OLR (bottom) in the 480LO-2 simulation, under initial condition (left of vertical line) and after evaporation is turned off at 120 days. ....	71
8.5	Domain-averaged (a) precipitation (top), (b) ARC (second from top), (c) SHF (second from bottom), and (d) net cooling (bottom) in the 480LO-2 simulation with evaporation turned off initially. ....	72

## CHAPTER 1

# ENERGETIC CONSTRAINTS ON THE HYDROLOGIC CYCLE

Precipitation is arguably one of the most important processes in the climate system, but it is also among the most complex; this complexity is apparent in the difficulty that most general circulation models (GCMs) have simulating precipitation and convective processes. Traditionally, precipitation has been considered in terms of the availability of moisture in the atmosphere. As many have suggested, however, in a warming climate, the rate at which the globally averaged precipitation rate increases does not match that of water vapor as seen in GCM projections (Allen and Ingram, 2002; Held and Soden, 2006). Whereas models have predicted that water vapor will scale with sea surface temperature (SST) according to the Clausius-Clapeyron equation at a rate of approximately  $7\% \text{ K}^{-1}$ , precipitation—as modeled by 19 GCMs in the Coupled Model Intercomparison Project 3—is projected to increase at a much slower rate, from  $1\text{-}3\% \text{ K}^{-1}$  (Figure 1.1).

This discrepancy has prompted a closer look at additional constraints on the hydrologic cycle that would limit precipitation growth beyond that of moisture availability alone—namely the atmospheric energy budget, which will be the focus of this paper. The relationship between the hydrologic cycle and the atmospheric energy budget is only valid, however, on appropriate spatial and temporal scales. Given that the hydrologic cycle of the climate system equilibrates over a period of months, it is reasonable that energetic constraints hold on the monthly time scale, and certainly on interannual and longer timescales on the global scales.

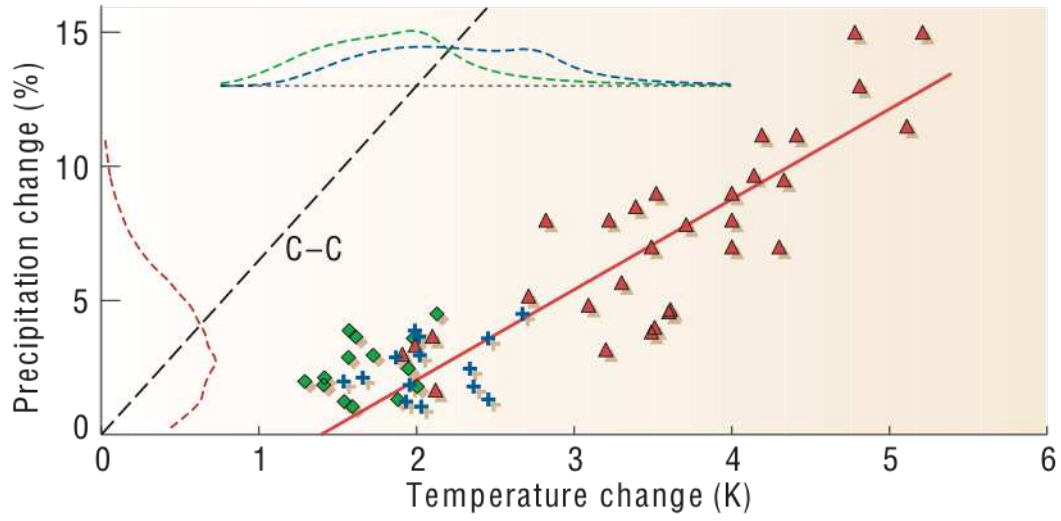


FIGURE 1.1. The rate at which precipitation increases (according to 10 GCM in CMIP3) differs greatly from that expected with the Clausius-Clapeyron approximation. From Allen and Ingram (2002).

First, consider precipitation in terms of energy, which can be written as the latent heat flux:

$$(1.1) \quad LE = L \cdot P,$$

where  $LE$  is the latent heat of condensation,  $L$  is the latent heat of vaporization of water, and  $P$  is the precipitation rate. On the global scale, horizontal energy transport vanishes and the global energy budget can be approximated as:

$$(1.2) \quad L \cdot P + SH = ARC,$$

where precipitation and the surface sensible heat flux ( $SH$ ) balance the  $ARC$ , the atmospheric radiative cooling. The  $ARC$  is defined as the radiative loss of energy by the atmosphere due to the fluxes of solar and terrestrial radiation across the earth's surface and the top-of-atmosphere. Although convention uses the diabatic heating rate,  $Q$ , the use of the  $ARC$  instead is convenient because it makes cooling a positive quantity. To consider the change of each of these quantities in a warming climate, it is easy to translate this budget equation into a perturbation equation:

$$(1.3) \quad L\delta P = \delta ARC - \delta SH.$$

How important is each term of equation 1.3 in regulating precipitation? Some argue that the sensible heat flux is too large to be ignored (Muller and O’Gorman, 2011; O’Gorman et al., 2012). In their analysis using an idealized GCM, they consider the balance between  $ARC$  and precipitation only in the free troposphere (above the lifting condensation level), removing the need to account for surface fluxes. Although they find that their approach

works well with simulated data (O’Gorman et al., 2012), this methodology cannot be easily applied to observational data due to the difficulty of measuring energy fluxes at specific vertical levels.

Alternatively, some argue that the energy constraint on precipitation is primarily radiative. Stephens and Ellis (2008) show that ARC is the primary component that drives precipitation, with a near one-to-one relationship between the global and annual means of each quantity using data that reflects the change over 70 years in CMIP3 models with a doubling of CO<sub>2</sub> (Figure 1.2). Nearly identical results were found in Vecchi and Soden (2007). Beyond acknowledging a primarily radiative constraint, Pendergrass and Hartmann (2014) suggest that the constraint is largely due to clear-sky ARC. Although clear-sky ARC alone does not balance precipitation, their analysis of analogous data from CMIP5 shows a correlation of 0.91 between the change in clear-sky ARC and precipitation (both scaled by SST change), suggesting that they do scale together quite strongly.

What is particularly interesting regarding the relationship between ARC and precipitation is that despite their strong positive relationship on the global scale (as required to maintain the atmosphere’s energy balance), the opposite relationship is found locally. Considering that a large portion of the globe is covered with convective clouds that produce precipitation, but decrease the ARC (due to a reduction in outgoing longwave radiation (OLR) by emitting at a lower temperature than the earth’s surface), this negative correlation on a regional scale makes sense. To investigate the scale-dependence of this relationship, Muller and O’Gorman (2011) looked at the correlation between the changes in ARC and precipitation (in 12 CMIP3 models between and the first and last 20 years of the A1B scenario<sup>1</sup>)

---

<sup>1</sup>According to the IPCC SRES Report, the A1B emissions scenario simulates a future world of very rapid economic growth, global population that peaks in mid-century and declines thereafter, and a balance between fossil-intensive and non-fossil energy sources; the estimated temperature change at the end of the 21<sup>st</sup> century is 2.8 C. The closest analog in the CMIP5 scenario is RCP 6.0.



as a function of the length scale. Their results show a negative correlation for small scales ( $10^2$  km) that becomes positive for scales near  $10^3$  km, and increases to unity for scales larger than  $10^4$  km.

Although the constraints on precipitation are straightforward on a global scale, the regional constraints are more complicated, due to the need to account for horizontal energy transport by large-scale circulations (Muller and O’Gorman, 2011). In a GCM study looking at the response at all locations of daily precipitation to  $\text{CO}_2$  doubling, it was observed that the highest end of the distribution consisted of all tropical locations and which increased by roughly 25%, which is more than would be expected from the Clausius-Clapeyron relationship of 22% (Allen and Ingram, 2002). Because the increases seen in the tropics are over double the increase in global-mean precipitation, this implies that precipitation must decrease in some regions to compensate. In general, the precipitation trend is to increase in regions where it is already high, and to decrease where evaporation is high (Manabe and Wetherald, 1980).

In a similar study comparing the tropical precipitation trend to that observed globally, but instead using observations from the Special Sensor Microwave Imager (SSM/I), it was shown that the increasing trend in the tropics was stronger than the trend over the entire globe (Wentz et al., 2007). However, one of the more interesting results from this study was that it showed precipitation increasing at the rate of approximately  $7\% \text{ K}^{-1}$ , much higher than that seen in any of the models.

Because constraints on tropical precipitation patterns and trends over the tropics as a whole are so complex, several studies decomposed the larger tropical region into areas of rising and subsiding air (Allan, 2006; Allan and Soden, 2007; Allan et al., 2010). By looking at the vertical velocity at 500 mb and decomposing the tropics into ascending and descending

regions, this produced more coherent trends than considering the tropics as a whole. Using observational data from the Global Precipitation Climatology Project (GPCP), the Climate Prediction Center Merged Analysis of Precipitation (CMAP), and SSM/I, they observed an increasing precipitation trend in ascending regions and the opposite in descending regions, supporting the popular wet-get-wetter (dry-get-drier) hypothesis of Held and Soden (2006). Unlike the observations, however, the simulations seem to show little to no trend in either ascending or descending regions over a 50-year period from 1950-2000. Adding to this uncertainty is a discrepancy between observational datasets, with SSM/I data showing a response nearly twice as large as that seen in with the GPCP data (Allen et al., 2010).

Because of the many discrepancies and high uncertainty among projections of future precipitation, and the burgeoning research using the atmospheric energy budget to constrain the precipitation, this study aims to answer several of the remaining questions that tie the hydrologic cycle to the energy budget. Specifically, we ask the following questions:

- (1) The connection between clouds and precipitation is generally well understood, but what is the effect of clouds on the ARC?
- (2) What is the seasonal relationship between precipitation and the ARC?
- (3) What is the regional relationship between precipitation and the ARC?

In the following chapter we use observational data to explore these questions. In Chapter 7, we use a cloud-resolving model to consider the relationship between the energy budget and the hydrologic cycle in the context of convective aggregation.

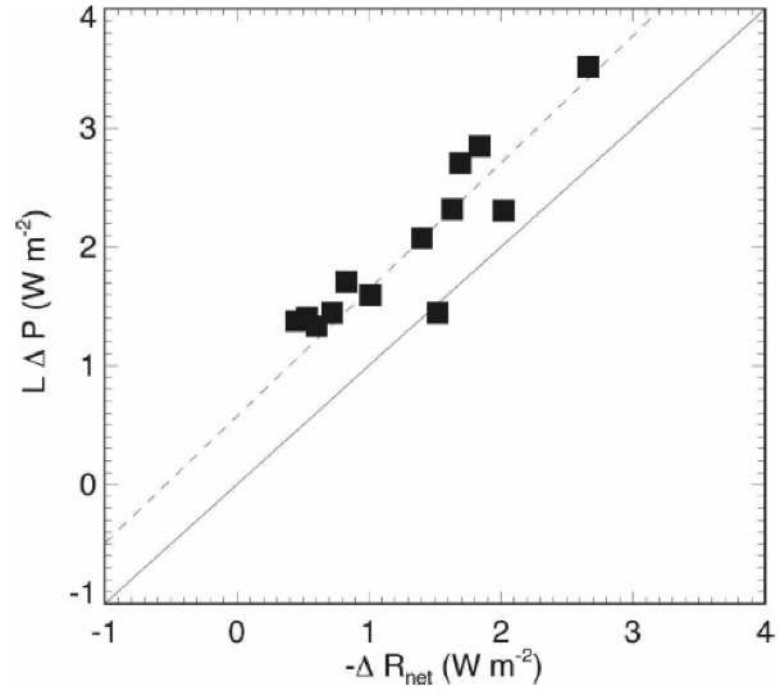


FIGURE 1.2. CMIP3 models show a strong positive relationship between the changes in latent heating and radiative cooling. From Stephens and Ellis, 2008.

## CHAPTER 2

# DATA AND METHODS

### 2.1. DATA

2.1.1. PRECIPITATION. Precipitation data from the Global Precipitation Climatology Project (GPCP) Version 2.2 was used in this analysis (GPCP Precipitation data provided by the NOAA/OAR/ESRL PSD, Boulder, Colorado, USA, from their web site at <http://www.esrl.noaa.gov/psd/>) (Adler et al., 2003; Huffman et al. 2009). The GPCP Version 2.2 dataset provides gridded monthly means from January 1979 to October 2015, though only dates through December 2014 were used.

The GPCP dataset is a joint project under the Global Energy and Water Cycle Exchange Project and the World Climate Research Program, and combines ground-based rain gauge observations with satellite measurements (of precipitation from both microwave and infrared sensors in combination with OLR measurements) for an integrated (blended) dataset. The data has a  $2.5^\circ$  latitude  $\times$   $2.5^\circ$  longitude resolution. Measurements have been better constrained since the introduction of the SSM/I sensor (years).

2.1.2. RADIATIVE FLUXES. Data from the Clouds and Earth’s Radiant Energy System (CERES) SYN1deg Product were used for global radiative fluxes (Wielicki et al., 1996). The SYN1deg product features CERES-observed geostationary enhanced temporally interpolated top-of-atmosphere (TOA) radiative fluxes at the TOA for all-sky and clear-sky conditions, and MODIS-derived and 3-hourly geostationary satellite cloud properties. Surface fluxes are computed using the Langley Fu-Liou radiative transfer model. The temporal scale of the fluxes used were monthly in scale, and the temporal resolution is  $1^\circ$  latitude  $\times$   $1^\circ$  longitude.

The following fluxes were obtained to calculate the ARC: solar insolation, outgoing longwave, and reflected solar at the TOA, and absorbed and reflected shortwave, and emitted and absorbed longwave at the surface. This product has only been available since March 2001. Clear-sky and all-sky data were used in comparison to investigate the role of clouds on the ARC.

## 2.2. METHODS

2.2.1. *ATMOSPHERIC RADIATIVE COOLING.* Atmospheric Radiative Cooling can be thought of as the diabatic heating rate, but conveniently for our purposes, defined so that cooling is positive. ARC is the net radiative loss of energy by the atmosphere due to solar and terrestrial radiation flowing across the atmosphere's top and bottom boundaries. We can define the ARC as:

$$(2.1) \quad \text{ARC} = (\text{LW}_{\text{TOA}} - \text{LW}_{\text{SFC}}) - (\text{SW}_{\text{TOA}} - \text{SW}_{\text{SFC}}),$$

where the four quantities are defined as the net flux at each level. As per convention, LW is defined as positive upward, and SW is defined as positive downward.

## CHAPTER 3

# OBSERVED RADIATIVE CONSTRAINTS ON THE HYDROLOGIC CYCLE

### 3.1. CLIMATOLOGY

3.1.1. PRECIPITATION. The long-term mean of the precipitation rate was mapped using GPCP observations of the monthly mean from 1979-2014, as shown in Figure 3.1. This plot shows strong agreement with previous GPCP analyses (version 1: Adler et al., 2003; version 2: Huffman et al., 2009) as well as older climatologies (Jaeger, 1976; Leages and Wilmott, 1990); minor differences are attributable to the extended time period of observations as well as improvements in both satellite and rain gauge data. Globally, the maximum precipitation is manifest as a strong band along the Intertropical Convergence Zone (ITCZ), spanning across the Atlantic, Pacific, and Indian Oceans, and broadening over the Indo-Pacific warm pool. Within this precipitation-laden region, the most precipitation over land occurs over the Maritime Continent and the Amazon, with high precipitation rates also observed in the Congo. Secondary maxima are found in the mid-latitudes along coastal storm tracks, stronger in the Northern Hemisphere (off North America and Asia) than in the Southern Hemisphere.

The driest regions over the oceans are found in the subtropics, largely off the western coasts, as well as over both poles. Over land, suppressed precipitation is also observed over regions with mountainous and desert terrain, corresponding to subtropical high pressure zones.

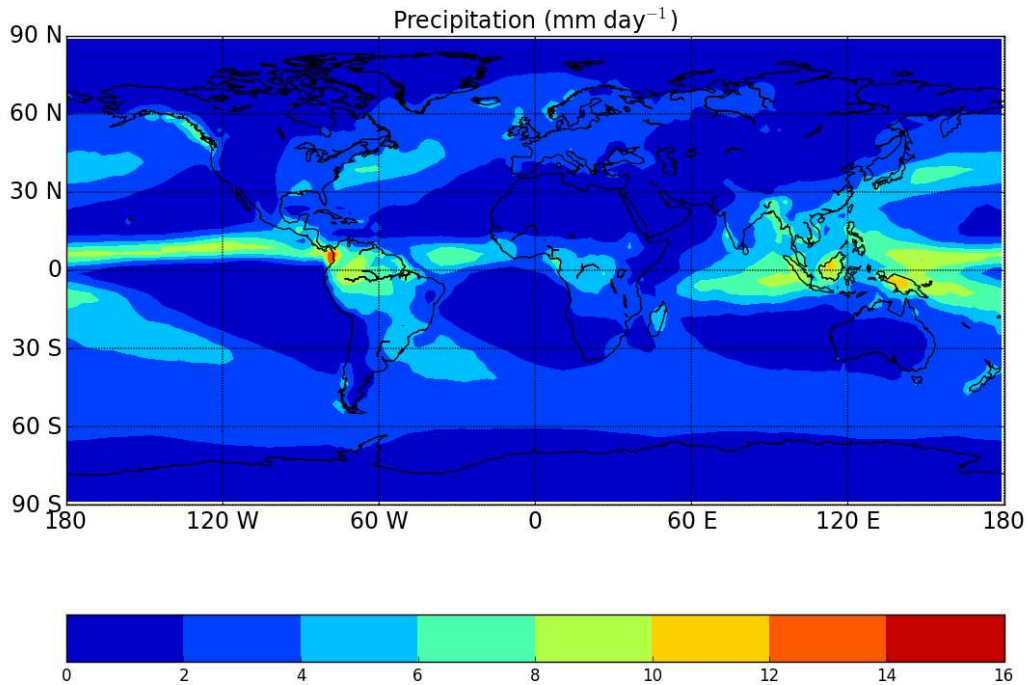


FIGURE 3.1. Precipitation climatology from GPCP monthly means (1979 - 2014).

3.1.2. ATMOSPHERIC RADIATIVE COOLING. Radiative flux measurements from 2001-2014 were used to calculate the ARC long-term mean. Figure 3.2a shows that the global ARC pattern is characterized by patches of high ARC in the Arctic and off the western coastlines in the subtropics, and in the Southern Hemisphere, reaching into the Tropics just south of the ITCZ. In the Tropics, the ITCZ and Indo-Pacific warm pool are marked by the ARC minima, and in general, continents show lower ARC than the oceans; this pattern can be partially explained by higher surface albedo over land, increasing upward shortwave fluxes at the surface. Some regions of low ARC appear to align with regions of enhanced precipitation.

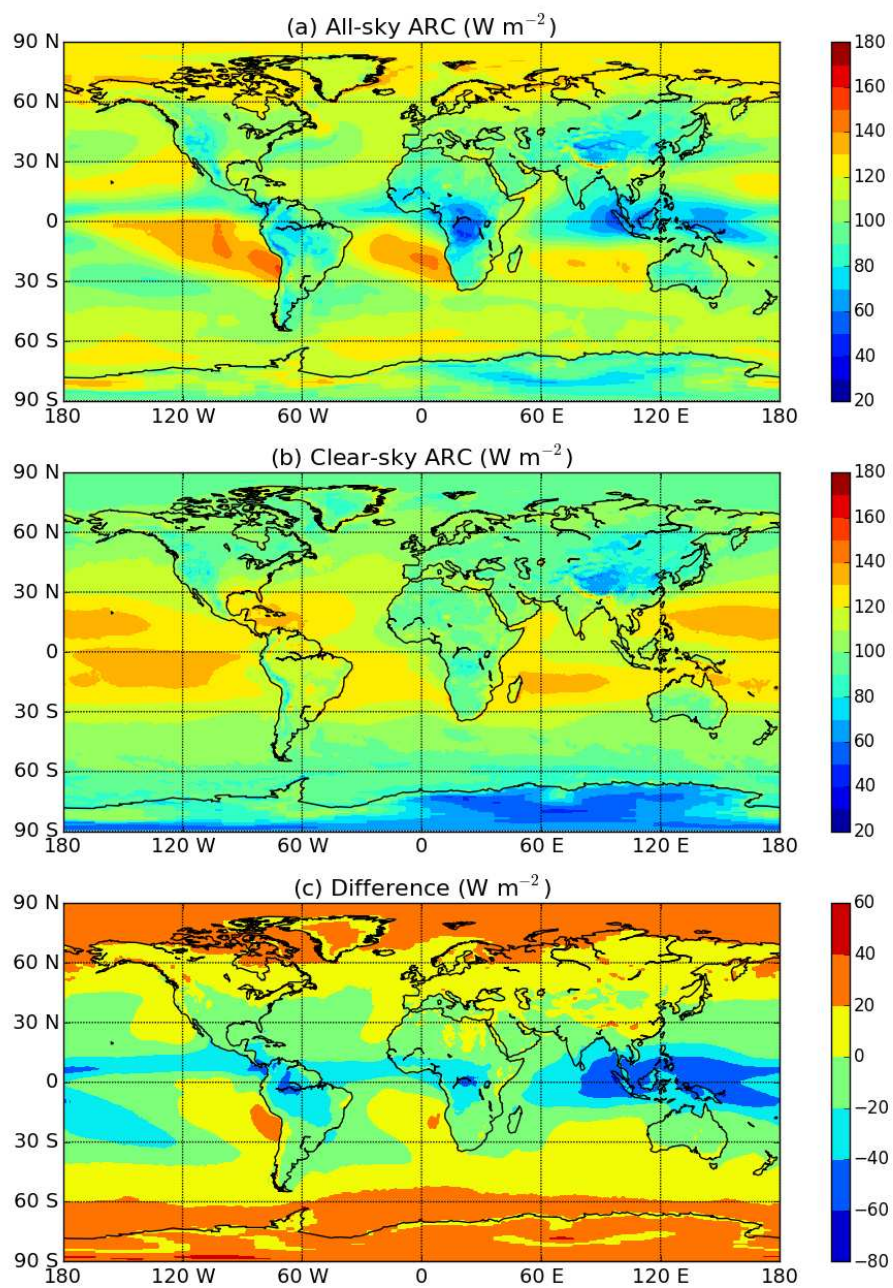


FIGURE 3.2. (a) all-sky ARC, (b) clear-sky ARC, (c) all-sky - clear-sky ARC. Climatology from CERES monthly means (2001 - 2014).



3.1.3. SEASONAL CYCLE. A comparison of the globally averaged long-term monthly means of the ARC and precipitation rates serves as a simple way to observe the annual cycle (Figure 3.3). From April to October, ARC and precipitation appear to be in-phase with each other, peaking during the summer. Where the precipitation rate is maximized over the months of June, July, and August, the ARC reaches a distinct maximum in July. Between the months of November and March, however, ARC and precipitation change in opposite directions. While the ARC reaches a minimum in March, the precipitation rate shows a distinct secondary maximum in the late winter. This discrepancy in the behavior of ARC and precipitation over half of the year suggests that the sensible heat flux must partially compensate for these changes, and also that the Northern and Southern Hemispheres behave separately. The extent of the relationship between precipitation and ARC on a regional scale is examined in section 3.3.

3.1.4. INTERANNUAL VARIABILITY. Because the annual cycles of both ARC and precipitation are largely dominated by seasonal variations, Figure 3.4 shows a time series of both fields with removed seasonality. The seasonal cycle was removed by subtracting out the annual composite, revealing that the ARC tends to exhibit both greater intra-annual and interannual variability than precipitation. The time series also serves to highlight the in-phase, out-of-phase cycle over the 14-year period.

## 3.2. EFFECTS OF CLOUDS

It is well known that precipitation is closely tied to the presence and location of clouds. Early attempts to quantify the relationship between tropical convective rainfall and clouds

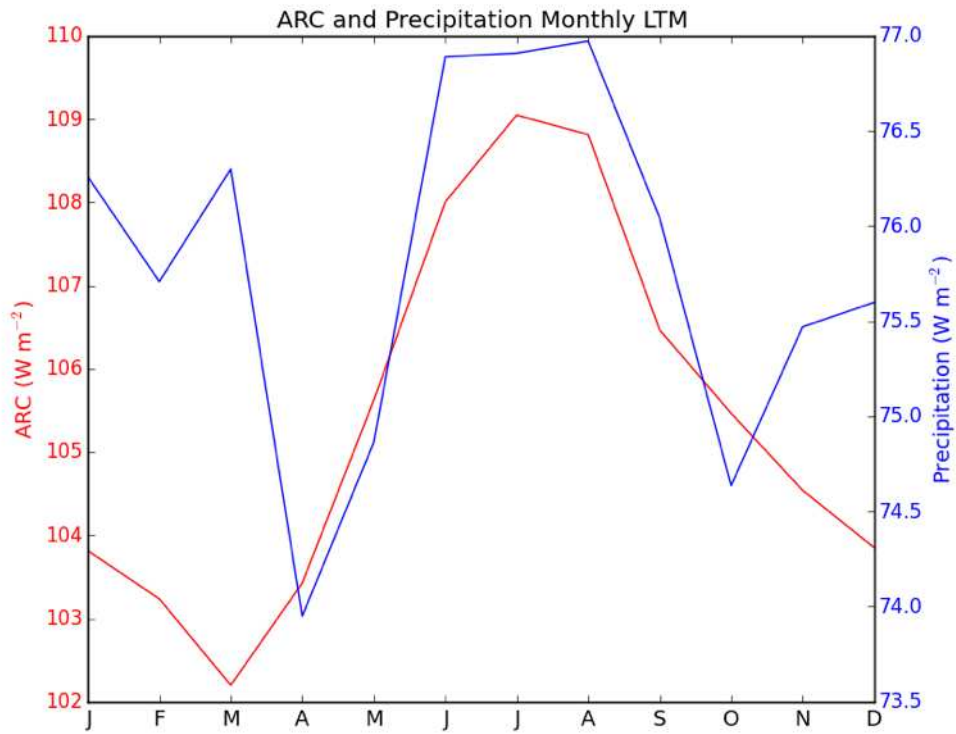


FIGURE 3.3. ARC and Precipitation seasonal cycle from monthly means.

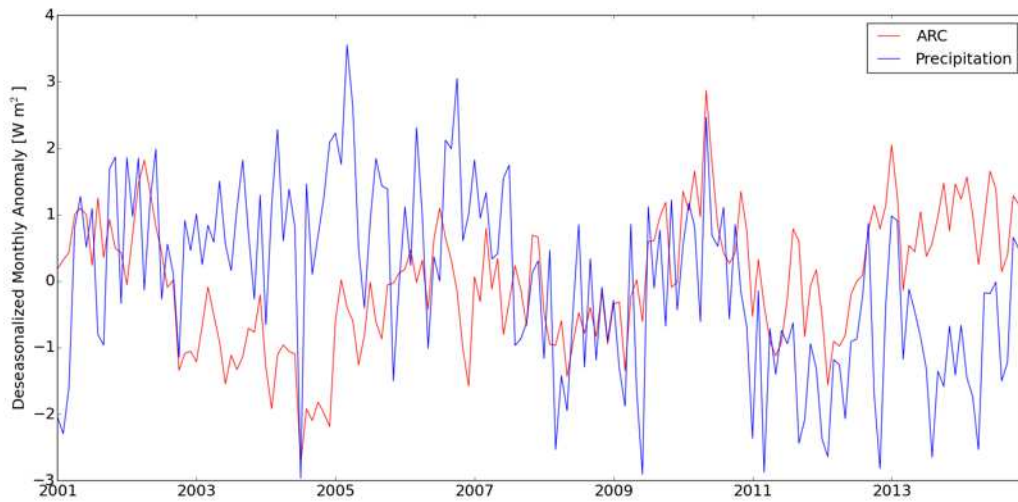


FIGURE 3.4. ARC and Precipitation interannual variability (deseasonalized).

first involved highly reflective clouds (Kilonsky and Ramage, 1976), and were later improved upon to find a stronger negative relationship between convective rainfall and OLR (Lau and Chan, 1983; Morrissey, 1986; Motell and Weare, 1987). An analysis by Xie and Arkin (1998) revealed how the correlation between precipitation and OLR changes from equator to pole: strongly negative in the tropics gradually becoming strongly positive near the poles, and showing a strong seasonal cycle in the mid-latitudes.

But how do clouds affect the ARC? The majority of research has focused on the effect of clouds on OLR, and although the OLR is closely related to the ARC, the inclusion of both shortwave fluxes and surface fluxes in the ARC sets the two fields apart. To answer this question, we use observations at the TOA and computed measurement at the surface.

Averaging over the entire globe, the all-sky long-term mean of ARC is only negligibly less than that of the clear-sky ARC long-term mean (105.36 versus 108.66  $\text{W m}^{-2}$ ), so that globally, the effects of clouds serve to decrease—albeit minimally—the ARC (i.e. warm the atmospheric column). In Figure 3.2, maps of the all-sky and clear-sky ARC climatologies show the regional effects of clouds on the ARC.

In the tropics, clouds generally act to reduce the ARC, especially near the equator. Regions of reduced ARC by clouds include the Amazon and the Congo—both tropical rainforests; this effect is also observed to a lesser degree in Southeast Asia and the Southeastern United States. The effect of clouds over the tropical ocean is more complex: clouds act to increase—and very strongly in the Southern Hemisphere—the ARC off the western coasts of continents due to the presence of marine stratocumulus decks (Lilly, 1968; Randall, 2012). Although they generally reduce the ARC near the equator—most noticeably across the Indian and western Pacific Oceans, as well as off the western coasts of South America and Africa, their effect is to increase the ARC.

In the mid-latitudes, the overall effect of clouds is weaker than that seen in the tropics. In the Southern hemisphere, clouds reduce the ARC over the continents and off eastern coasts, while increasing the ARC off the western coasts. In the Northern hemisphere, the effect of clouds is to increase ARC over both ocean and land, and this cooling effect becomes stronger moving poleward. At high latitudes, clouds increase the ARC and have a strong cooling effect over both land and ocean.

3.2.1. ARC COMPONENTS. Figure 3.5 shows the zonally-averaged effect of clouds on the ARC, but also examines the effects on the upper and lower boundaries of the atmosphere, and differentiates between the longwave and shortwave response. Clouds act to decrease ARC in the Tropics, which is attributed to decreased OLR. At higher latitudes, clouds act to increase ARC due to an increase in reflected shortwave radiation, and also serve to increase downwelling longwave radiation near the poles and in the subtropics. The radiative effect of clouds on the ARC appears to be dominated by changes in longwave cooling, though the pattern is enhanced by changes in downwelling radiation at the surface.

### 3.3. SEASONAL CORRELATIONS

A map of the temporal (seasonal) correlation between monthly means (2001 - 2014) of the ARC and precipitation is incredibly revealing (Figure 3.6). Although the continents do tend to favor a negative correlation, the most striking feature of the map is that most of the tropics are characterized by a negative correlation—the strongest of which appears near the equator and western Pacific warm pool—whereas poleward of  $30^\circ$ , the correlation is mostly positive, with some exceptions over land in the northern hemisphere, where inland North America and Russia exhibit a negative correlation.

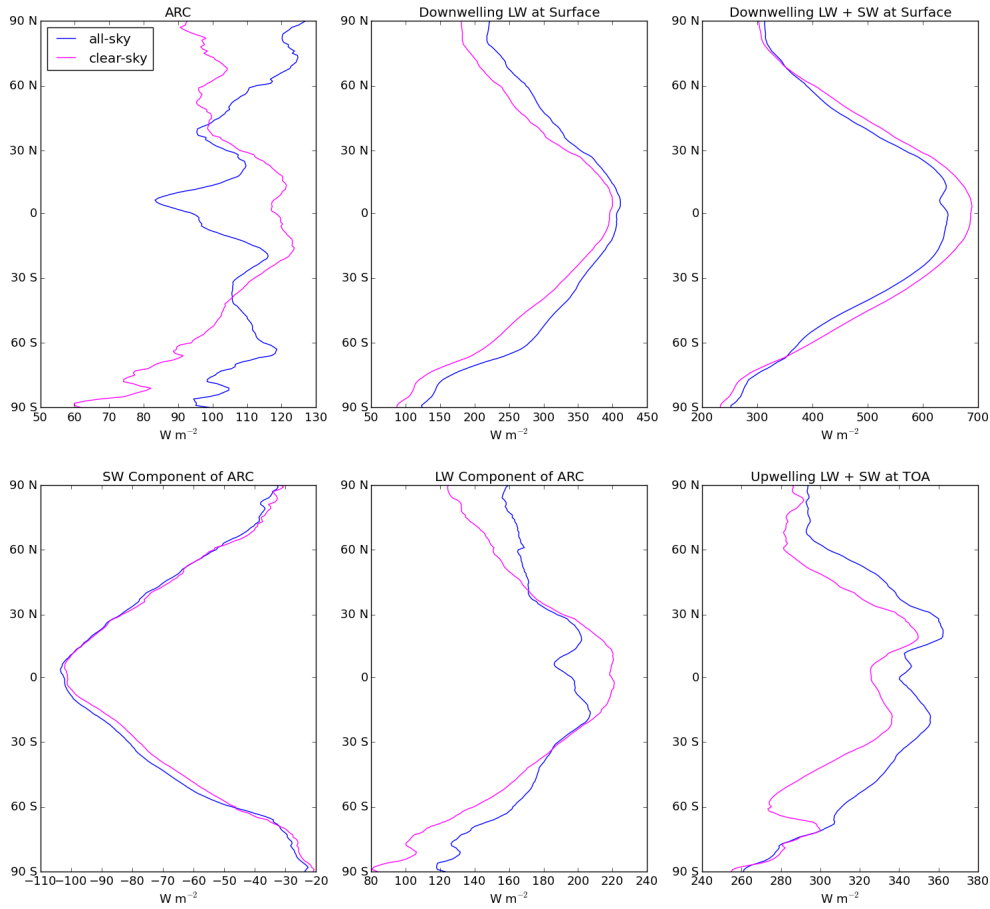


FIGURE 3.5. Radiative effect of clouds on the total ARC and on ARC components.

To simplify the correlation map and look at the how ARC and precipitation relate to each other zonally, we look at a plot of the zonally-averaged seasonal correlation (Figure 3.7a) the seasonal correlation of zonal averages (Figure 3.7b). Figure 3.7a shows a maximum negative correlation of approximately -0.6 on either side of the equator, and a steady increase in correlation through the mid-latitudes. Near 40° N and S, the correlation becomes positive, eventually reaching a maximum near 60° S and 90° N, though the maximum correlation is not nearly as strong.

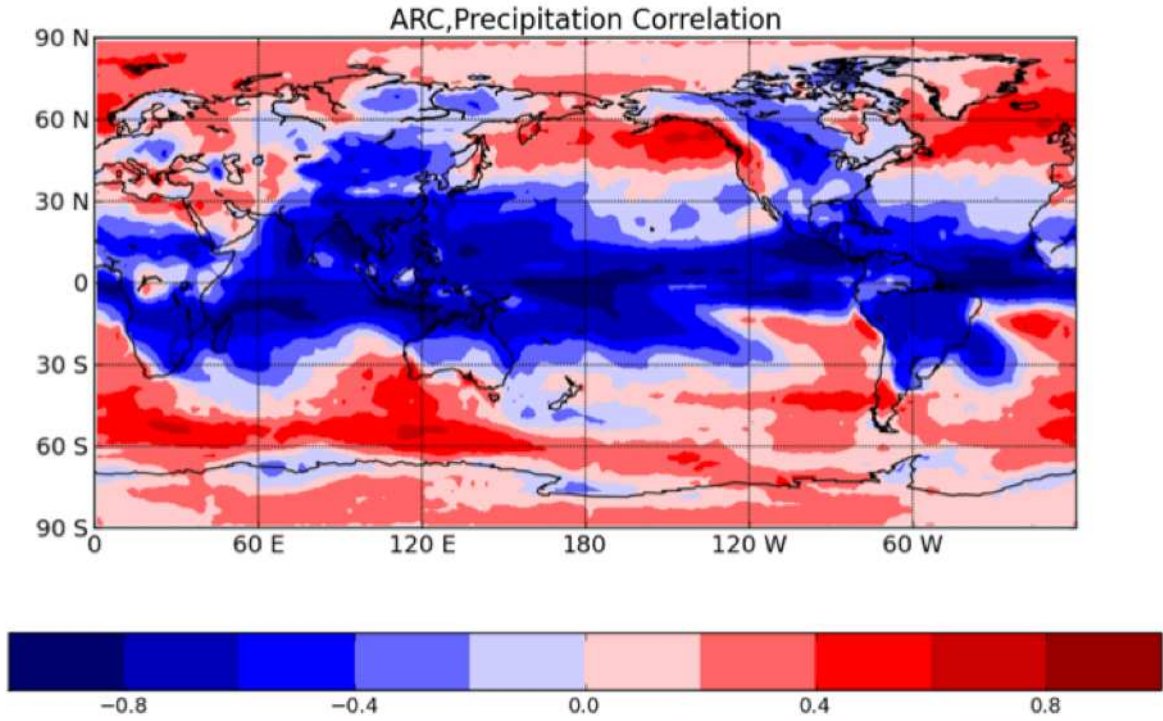


FIGURE 3.6. Seasonal correlation between ARC and precipitation using monthly means.

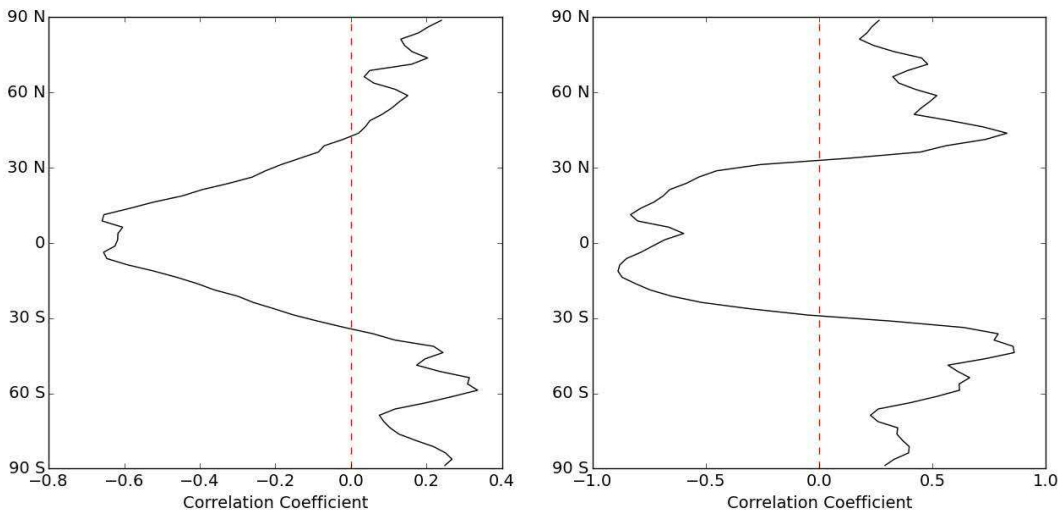


FIGURE 3.7. (a) Zonally averaged correlation of ARC and precipitation (left), (b) Correlation of zonally averaged ARC and precipitation (right).

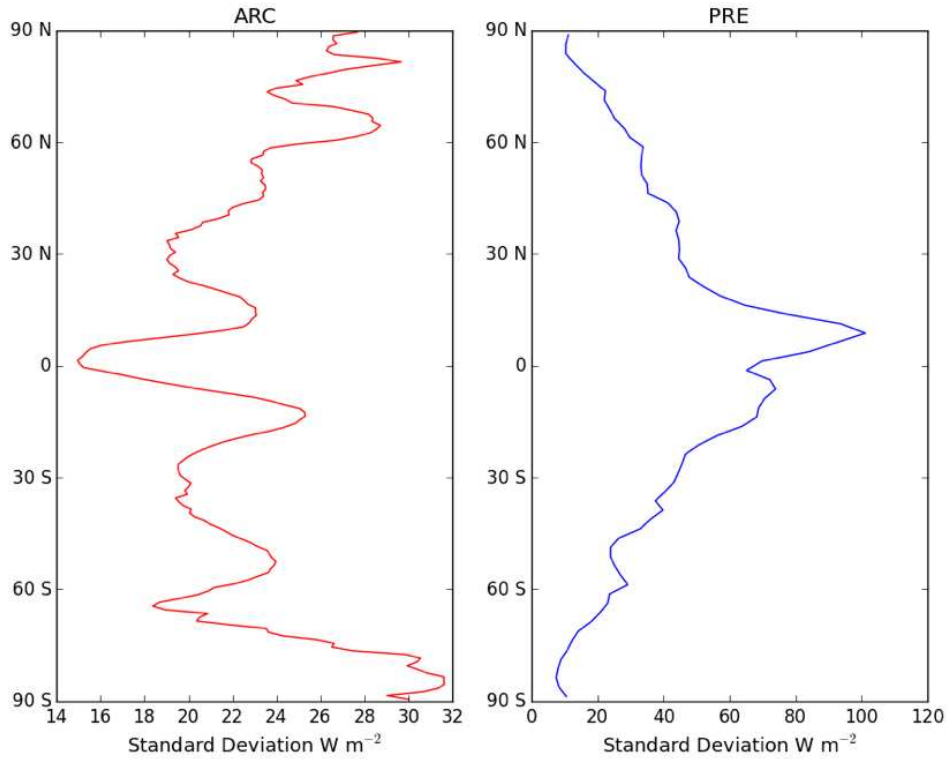


FIGURE 3.8. Zonally averaged standard deviants of (a) ARC (left) and (b) Precipitation (right).

Figure 3.7b is more striking than Figure 3.7a, and features a stronger negative correlation in the tropics that sharply changes to a positive correlation near  $30^\circ$  N and S. The negative correlation in the tropics reaches a maximum of  $-0.8$  at approximately  $15^\circ$ , but reaches a local minimum just north of the equator. Poleward of the two local tropical maxima, there is a sharp change in the correlation that then increases to  $0.8$  near  $40^\circ$  N and S where it reaches a local positive maximum followed by a slow decrease as it approaches the poles in both hemispheres. Further explanation of the zonal structure of the correlation can be drawn from the zonally-averaged temporal standard deviations of each field (Figure 3.8); where we expect to see a high correlation where the standard deviation is low.

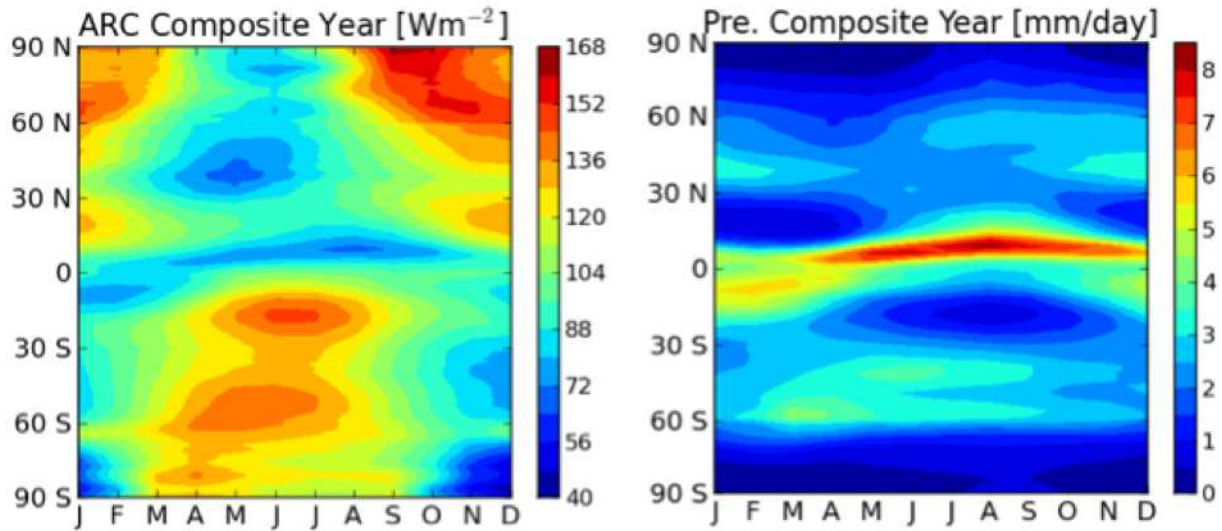


FIGURE 3.9. The zonally averaged seasonal composite of (a) ARC (left) and (b) Precipitation (right).

To better understand the abrupt change in the sign of the correlation, we compare composited zonal averages throughout the year. Figure 3.9a shows the ARC composite year, exhibiting a general pattern of stronger cooling in the Northern Hemisphere (NH) than in the Southern Hemisphere (SH) when comparing both NH and SH summers and winters to each other. The NH fall/winter season is marked by a maximum in ARC, especially near the poles. In general, cooling is stronger in the winter than in the summer in both hemispheres.

Looking at the composite year for precipitation (Figure 3.9b), the NH and SH are largely more symmetric than the ARC; the hemispheres are still affected by seasonality, but to a lesser degree. Precipitation is maximized in the summer months near the equator in both hemispheres, but the NH exhibits a stronger maximum than that in the SH. Along those lines, both hemispheres show increases in the subtropics in fall/winter, but the SH exhibits a stronger increase than the NH.



Comparing these two plots provides some insight as to why the correlation has the zonal structure that it does. In the ITCZ, both ARC and precipitation experience strong fluctuations throughout the year: when precipitation is maximized, ARC is minimized (during the summer in each hemisphere). At higher latitudes poleward of  $30^\circ$ , however, they tend to change together, causing the near 1.0 correlation just above  $30^\circ$  N and S. At latitudes higher than  $30^\circ$ , however, the correlation gradually loses strength all the way to the poles. This can be attributed to the fact that poleward of  $75^\circ$ , the precipitation remains very low throughout the year, whereas the ARC undergoes large seasonal changes.

### 3.4. CONCLUSIONS

Comparing the global averages of ARC and precipitation throughout the year, the two fields appear in-phase during NH summer and out-of-phase during NH winter; this suggests a seasonal hemisphere-dependence. A composite of the zonal means shows that the zonally averaged precipitation rate remains relatively steady throughout the year, but the ARC undergoes strong seasonal shifts in each hemisphere. Combined, these patterns produce a strong negative correlation between precipitation and the ARC in the tropics, and a positive correlation at mid- and high latitudes. Although Pendergrass and Hartmann (2014) suggest that the radiative constrain on precipitation is dominated by the clear-sky ARC, our results suggest that the precipitation and all-sky ARC are strongly related.

Interestingly, the sign of the correlation appears to be related to the sign of the effect of clouds on the ARC. In the tropics, where clouds act to reduce the ARC, the correlation is negative, and at higher latitudes, where clouds act to increase the ARC, the correlation is positive. The radiative effect of clouds on the ARC appears to be dominated by changes in longwave cooling.

## CHAPTER 4

### BRIDGE

Although the evidence for the relationship between the atmospheric energy budget and the hydrologic cycle is strong, the way they will affect each other in the future is not fully clear. As stated in Held and Soden (2006), GCMs project an increase of approximately 2%  $\text{K}^{-1}$  in the precipitation rate, whereas water vapor increases at a much higher rate (in line with Clausius-Clapeyron), near 7%  $\text{K}^{-1}$ ; this difference is attributed to the constraint of atmospheric energetics on the hydrologic cycle.

Although there are satellite observations of precipitation dating back to 1979, observational analyses of the trend in precipitation over time vary widely due the array of datasets that both directly (and indirectly) measure the precipitation rate, and do not readily agree with GCMs. The global average linear change in GPCP v2.1 data shows a nearly imperceptible change of  $+0.0069 \text{ mm day}^{-1} \text{ decade}^{-1}$  over the entire study period (1979 - 2007), and a slightly larger change of  $+0.0169 \text{ mm day}^{-1} \text{ decade}^{-1}$  for just the SSM/I era (1988 - 2007) (Huffman et al., 2009). Using the GPCP v2.1 global mean of  $2.68 \text{ mm day}^{-1}$  and a warming of  $0.2 \text{ K decade}^{-1}$ , these rates correspond to changes of  $0.01\% \text{ K}^{-1}$  and  $0.03\% \text{ K}^{-1}$ , respectively. Looking at precipitation over land exclusively, observational datasets show a wide spread in the magnitude of the change in precipitation, and do not even agree on the sign of the change over the second half of the 20th century (Hartmann et al., 2013). Some datasets, however, show growth in the precipitation rate that far exceeds the  $2\% \text{ K}^{-1}$  of the GCMs. Wentz et al. (2007) first showed a heightened trend using the Special Sensor Microwave Imager (SSM/I) with global coverage from 1987 to 2006 (Figure 4.1). The data showed a trend of  $6\% \text{ K}^{-1}$  (using a warming of  $0.2 \text{ K per decade}$ ), which unlike the GPCP data, is

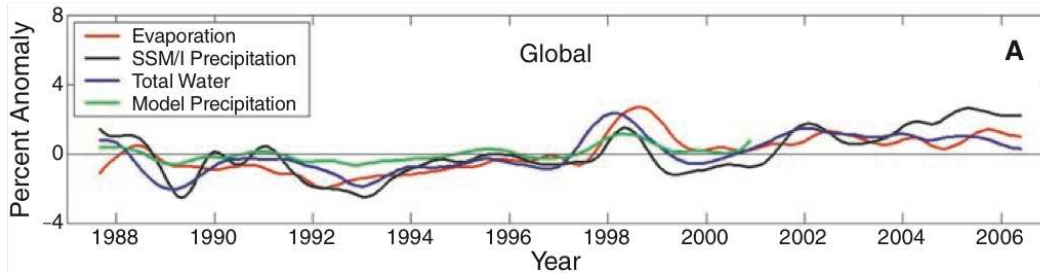


FIGURE 4.1. The change in the percent anomaly of the global mean SSM/I precipitation rate is shown by the black curve. From Wentz et al., 2007.

more closely aligned with the water vapor increase expected with Clausius-Clapeyron. More recently, Durack et al. (2012) found that sea surface salinity patterns intensify by  $16\% \text{ K}^{-1}$  using observations from 1950 - 2000 (Figure 4.2). From this trend, coupled with a relationship between changes in sea surface salinity and changes in the surface evaporation and precipitation rates (determined by CMIP3 simulations), Durack et al. (2012) inferred that the hydrologic cycle had experienced amplification of  $4\%$  over the 50-year period, and that an amplification of  $8\% \text{ K}^{-1}$  could be expected in the future, given the  $0.5 \text{ K}$  warming over the last 50 years of the 20th century (Trenberth et al., 2007).

What do these observed trends of stronger precipitation and an amplified water cycle imply? Mauritsen and Stevens (2015) suggest that because GCMs do not explicitly resolve convection (and precipitation), there is the possibility that convective parameterizations in GCMs have produced unrealistically small precipitation increases with warming. They proposed that the missing link in these convective parameterization schemes is organized convection. In particular, aggregated convection is the process by which homogeneously distributed convection will spontaneously aggregate into a single patch of convective activity. As the moisture clusters together to produce small convective clusters, these eventually aggregate into a single large cluster of deep convective activity, with increased precipitation overall.

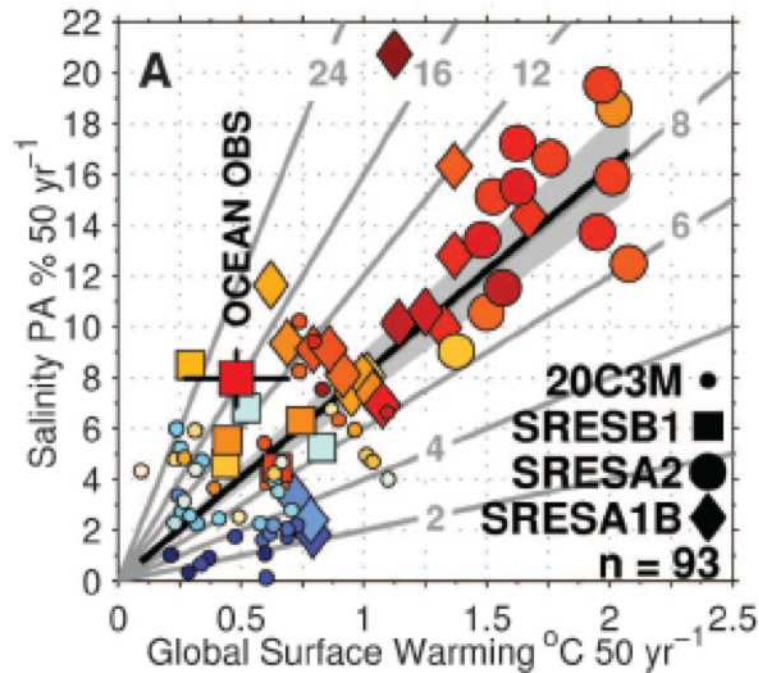


FIGURE 4.2. Correlation between the pattern amplification of Sea Surface Salinity and the the change in SST. From Durack et al., 2012.

Mauritsen and Stevens (2015) also shed a new light on the controversial Iris Hypothesis (Lindzen et al., 2001). The Iris Hypothesis posits an inverse relationship between the area of high cloud cover and the mean SST of cloudy regions, so that that as SSTs warm, cirrus cover decreases. An analysis of observational data by Lindzen et al. (2001) supported the hypothesis, and they concluded that with reduced cirrus cover, more energy can escape through an increased area of dry (clear) regions, acting as a negative feedback to cool the surface.

The bimodality of water vapor in the tropics—a function of shorter drying times than mixing times, so that drying dominates despite mixing of water vapor—is well documented and readily observable (e.g. Zhang et al., 2003). The distribution of dry and moist areas, and how they align with regions of cloudiness, motivated Lindzen et al. (2001) to examine how clouds act to moisten the regions around them.

The paper of Lindzen et al. (2001) received severe criticism for both its methodology (Fu et al., 2001; Hartmann and Michelson, 2002) and its assumptions (Lin et al., 2002). Furthermore, although Lindzen et al. (2001) suggested that increased precipitation efficiency could reduce cirrus detrainment, the hypothesis was largely dismissed because no mechanism for the adaptive iris was offered. Following the advent of the Iris Hypothesis, several studies looked into the validity of the temperature-dependence of precipitation efficiency. Rapp et al. (2005) found that although precipitation efficiency and cloud cover do appear to correlate with SST in warm clouds, the same cannot be said for deep convective systems. Their results were in agreement with Lau and Wu (1993), who found that in deep clouds, precipitation efficiency is controlled by the strength of updrafts as opposed to SST. These findings were inconsistent with those of Del Genio and Kovari (2002), in which precipitation efficiency was found to increase with increasing SSTs in tropical convection.

Mauritsen and Stevens (2015) suggested the possibility of convective aggregation as the mechanism behind the Iris Hypothesis, and that with its incorporation in GCMs, the gap between the precipitation trends in observations and simulations might close. To account for precipitation efficiency in convective parameterizations used in CGMs, Mauritsen and Stevens (2015) developed a simple model that includes a parameter to control the strength of the Iris Effect to represent the conversion of cloud water to rain,  $C_p$  (i.e. precipitation efficiency):

$$(4.1) \quad C_p(T_s) = C_0 (1 + I_e)^{T_s - T_0}$$

where  $C_0 = 2 \times 10^{-4} \text{ s}^{-1}$  (the default conversion rate in ECHAM6),  $T_s$  is surface temperature, and  $T_0$  is the reference temperature of 25° C. In this equation, the parameter  $I_e$  controls

the strength of the iris effect and is assigned values ranging from 0.2 to 1.0. Although precipitation efficiency is difficult to observe in nature, CRMs have the capability to compute precipitation efficiency because they resolve precipitation, as opposed to parameterizing it. Not only can CRMs calculate precipitation efficiency, but they are also widely used to model convective aggregation. In the context of convective parameterizations in GCMs and the associated microphysical processes, precipitation efficiency is calculated as the ratio of surface precipitation to the condensation rate.

Aggregated convection affects the atmospheric energy budget in that as the convection aggregates and high cloud amount is reduced, the increase in OLR is (at least partially) balanced by an increase in SW radiation at the surface. Mauritsen and Stevens (2015) compared the equilibrium climate sensitivity (ECS, the expected equilibrium surface warming associated with a doubling of atmospheric CO<sub>2</sub> concentrations), and found that the ECS was only mildly affected by accounting for the Iris Hypothesis, dropping from 2.8 K to 2.2 - 2.5 K. Although the ECS does not undergo a dramatic change, as the majority of the domain experiences extreme drying, this change in the domain-averaged moisture leads to increased OLR, which is then reflected in the ARC. Observational evidence has shown that convective clusters are characterized by increased precipitation efficiency (Tobin et al., 2012). Using a CRM to examine the effects of self-organized convection on precipitation is a natural next step. One study (Muller et al., 2011) explored the radiative constraint on the hydrologic cycle in a CRM by running two simulations with different SSTs of 300 and 305 K, but sharing the same prescribed ARC profile from the control (300 K) simulation. By increasing only the SST and keeping the ARC profile constant, the precipitation changed by less than 0.8% K<sup>-1</sup>, as expected, though precipitation extremes were found to change by 5.6% K<sup>-1</sup>,

suggesting that although the large-scale mean precipitation is generally dominated by global energetics, precipitation extremes are at the will of local dynamical processes.

Our study aims to provide a more in-depth examination of the radiative constraint on precipitation using a CRM, and in the context of aggregated convection. Additionally, we propose a hypothesis: that convective aggregation occurs where the radiative effect of clouds is to reduce the ARC, and that convective aggregation does not occur where the radiative effect of clouds is to increase the ARC. Our results in Chapter 3 show that the radiative effect of clouds is to reduce the ARC in the warm, humid tropics, which as shown in a number of previous studies (Khairoutdinov and Emanuel, 2010; Emanuel et al., 2013; Wing and Emanuel, 2014), are the conditions in which convective aggregation is favored. If aggregation only occurs where clouds act to reduce the ARC, then this also coincides with the region in which precipitation and the ARC are negatively correlated. Therefore, the discontinuities in the temporal correlation seen in Figure 3.7 at 30° N and S suggest that aggregation “switches” on equatorward of those latitudes, which would be expected if aggregation is a mode of instability that only occurs at sufficiently warm SSTs. We investigate this hypothesis in Chapter 7.

## CHAPTER 5

# SUMMARY OF PREVIOUS WORK ON AGGREGATED CONVECTION

Convective self-aggregation is the process by which deep convection spontaneously organizes into one or more isolated clusters without the assistance of external forcings, such as sea-surface temperature (SST) gradients or wind-shear. It has most actively been studied using CRMs. Some consider convective aggregation to be an example of radiative-convective instability, exhibiting a bifurcation of the traditional radiative-convective equilibrium into moist and dry states (Emanuel et al., 2013). Organized convection is known to occur in nature—on scales as small as squall lines and as large as the Madden-Julian Oscillation (Madden and Julian, 1971), and cloud clusters of varying sizes in the western Pacific warm pool (Mapes and Houze, 1993)—but the investigation of how simulated aggregated convection connects to observed organized convection is still in progress.

Convective aggregation starts with the development of a single dry patch in the midst of previously homogeneous convection. As the dry patch expands, convection is ultimately confined to a single cluster. This results in both increased OLR, which in turn increases the ARC, and increased precipitation. An overview of possible mechanisms behind convective self-aggregation, and its evolution, maintenance, and sensitivities is given below.



## 5.1. HYSTERESIS

Several studies have suggested that convective aggregation exhibits hysteresis: that aggregated convection can remain aggregated even if conditions become unfavorable (Khairoutdinov and Emanuel, 2010; Muller and Held, 2012). Although it has generally been found that convective aggregation in CRMs requires a sufficiently warm SST to develop, Khairoutdinov and Emanuel (2010) showed that once convection aggregated, the SST sensitivity was removed. Using a 2-m deep slab ocean model in which SST can fluctuate in response to surface fluxes, convective aggregation persisted even after reduced shortwave heating caused the SST to fall well below the critical SST. The inhospitable dryness of the subsiding region (covering the majority of the domain) explains why new convection cannot develop there, even though the existing aggregated convective activity can persist in its humid “nest”.

Following this initial study showing hysteresis of convective aggregation, Muller and Held (2012) further tested the idea that convection aggregation exhibits hysteresis by running simulations starting from already aggregated initial conditions, but testing for sensitivity to resolution as opposed to SST. The resolution sensitivity stems from increased cloud condensate at coarser resolutions (Khairoutdinov et al., 2009) and thus enhanced longwave cooling from low clouds (Muller and Held, 2012). In this scenario, a range of resolutions (the finest of which was 500 m) were found to maintain aggregation above a suitable domain size ( $L > 200$  km), even when such high resolutions could not support the development of convective aggregation from unfavorable homogeneously convective conditions. The fact that convective aggregation exhibits hysteresis suggests that there are separate mechanisms responsible for the development of self-aggregation and the maintenance of convective aggregation.

Furthermore, that convective aggregation can persist even when conditions are not favorable for the onset of aggregation lends credibility to the idea that aggregation may occur in nature, where conditions are far from idealized and can quickly change from favorable to unfavorable.

## 5.2. SENSITIVITIES

5.2.1. SEA SURFACE TEMPERATURE. The sensitivity of convective aggregation to SST has been extensively studied, but is still under debate. Khairoutdinov and Emanuel (2010) were the first to investigate a SST dependence by testing the response of convection to a range of fixed SSTs from 293 to 304 K; their results showed that a SST of at least 298 K was necessary for convection to aggregate into a single cluster. A recent, more comprehensive investigation of SST sensitivity was completed in Wing and Emanuel (2014), with simulations run from 297 to 312 K. In agreement with Khairoutdinov and Emanuel (2010), convective aggregation did not occur below a minimum temperature, in this case, 301 K. An unexpected finding, however, was that of an apparent maximum critical temperature, evidenced by the lack of aggregation in the 310, 311, and 312 K simulations, which they suggested might indicate that higher SSTs require a larger domain in order for self-aggregation to occur. Furthermore, not only was there a SST dependence for the occurrence of aggregation, but also for the type of aggregation: either banded or circular.

Emanuel et al. (2013) suggest that the temperature dependence is connected to the heating and cooling of the atmosphere in response to a decrease in humidity at all vertical levels. The upper tropospheric heating response to decreased humidity is weaker cooling, for all SSTs, while the lower tropospheric response, which is dominated by the longwave

response, varies with SST. The temperature dependence of the longwave heating response can be explained by the importance of water vapor to longwave emission, coupled with temperature dependence of water vapor given by the Clausius-Clapeyron equation. At lower SSTs (25° and 30° C), the response to a drying perturbation is weaker cooling in the lower troposphere, whereas the response at higher SSTs (35°, 40° and 45° C) is increased cooling of the lower troposphere. Therefore, only at high SSTs does the heating response to a reduced humidity act to increase the linear instability of the RCE state.

Although most modeling studies have concluded that warm SSTs are a prerequisite for convective aggregation, one observational study has provided evidence to the contrary. Tobin et al. (2013) suggest that the absence of a SST threshold in observations could be the result of gravity waves which act to homogenize atmospheric temperatures, a process that might be prevented in the limited domains found in CRMs, but that could occur in larger domains. Surprisingly, however, one modeling study of convection at extremely cold temperatures showed that convective aggregation occurred at temperatures as low as 243 K, possibly due to either the lack of cold pools at such low temperatures, or strong longwave cooling in dry regions (Abbot, 2014).

Because we are interested in investigating convective aggregation under current conditions and those associated with a warmer future, we will limit the SSTs used in the simulations to those that can be currently observed (even if they are rare for the time being), and have had success in producing convective aggregation across a number of studies.

5.2.2. DOMAIN SIZE AND RESOLUTION. Early work using 3D CRMs to investigate convective aggregation found that there is indeed a sensitivity to domain size; while aggregation occurs in large domains ( $L = 576$  km), convection remains disorganized in domains smaller

than that (Bretherton et al., 2005; Khairoutdinov and Emanuel, 2010). These simulations were run using 3 km grid-spacing. Later work, however, sought to determine if convection could aggregate with smaller domains by running a number of simulations with various combinations of domain size and resolution. Muller and Held (2012) found that by coarsening the resolution, aggregation occurred in domains as small as  $L = 200$  km. Furthermore, they found that aggregation was also dependent on resolution and that regardless of a favorable domain size, aggregation did not occur in simulations with grid spacings finer than 2 km. More recently, however, Jeevanjee and Romps (2013) found that cold pools were responsible for the domain-size sensitivity, and that when cold-pools were inhibited there was no lower threshold in domain size. Although aggregation occurred in smaller domains, it did appear that self-aggregation was weakened, as indicated by using minimum boundary layer specific humidity as a measure of the aggregation strength. They suggest that the dependence of aggregation strength on domain size can be explained by a secondary shallow circulation. In our simulations, we follow previous studies in which convective aggregation developed and begin with a domain of 768 km, followed by a domain of 480 km, which was still large enough to allow aggregation at our temperatures. For both domain sizes, a grid spacing of 3 km is used.

5.2.3. COLD POOLS. In an investigation of the role of the boundary layer in convective aggregation, Jeevanjee and Romps (2013) found that cold pools were responsible for this domain size threshold. In simulations where cold pools were suppressed by turning off evaporation of precipitation in the lowest 1000 m, aggregation occurred in domains as small as  $L \sim 100$ -200 km, though the strength of the aggregation was much weaker than that of larger domains. When cold pools were reintroduced, however, convection diasgregated

as the boundary layer of the dry region moistened, followed by the moistening of the free troposphere from deepened convection. From these experiments they concluded that larger domains not only allow for drier dry regions, but that cold pools must extend further in order to evenly distribute moisture, which keeps the dry region dry and maintains the single cluster of convective activity. In contrast to these findings, Muller and Held (2012) found that surface evaporation enhanced the necessary up-gradient transport of moist static energy (MSE), thus functioning as a positive feedback on convective aggregation. In Chapter 8, we discuss a new sensitivity to cold pools that we uncover during our initial series of sensitivity tests.

### 5.3. POSSIBLE MECHANISMS

5.3.1. A SECONDARY CIRCULATION. Analysis of the streamfunctions of two-dimensional aggregated convection over a range of domain sizes without cold pools (Jeevanjee and Romps, 2013) showed a clear division between a primary deep, dry circulation and a secondary shallow, moist circulation (respectively above and below 3500 m), supporting similar findings in Bretherton et al. (2005) and Muller and Held (2012). Whereas the shallow circulation increased weakly with increasing domain size, the magnitude of the deep circulation increased more strongly with increasing domain size, thus out-competing the shallow circulation in large domains. The different response of these circulations to increasing domain-size can explain the domain-size dependence of convective aggregation: in small domains, the shallow circulation dominates over the deep circulation by moistening the dry, non-convecting region and homogenizing the moisture between the two regions.

5.3.2. MOIST STATIC ENERGY TRANSPORT. An alternative mechanism involves the transport of MSE. Following Bretherton et al. (2005), Muller and Held (2012) analyzed streamfunctions in  $z$  and energy-space to investigate MSE transport between dry and moist regions. In domains characterized by convective aggregation, the shallow circulation—whose presence can be attributed to the low-level cooling due to low clouds in the dry region—was found to transport MSE up-gradient, from dry to moist regions, consistent with Bretherton et al. (2005). They found that the up-gradient transport was a result of strong longwave cooling, and that when longwave cooling (from the lowest 1 km) was removed convective clusters disaggregated. From this finding they conclude that the sensitivity of convective aggregation to both domain size and resolution can be tied to a CRM’s representation of low clouds.

## 5.4. ROLE OF RADIATIVE AND SURFACE FLUXES

5.4.1. SHORTWAVE FLUXES. To better understand the interaction between convection and radiative fluxes, a number of studies have suppressed interactive radiation by horizontally homogenizing fluxes at each vertical level and time step. In Muller and Held (2012), homogenizing shortwave fluxes had little effect on the ability of convection to organize, though several runs with homogenized shortwave fluxes did aggregate when they had not previously. Accordingly, they proposed that SW fluxes act to oppose aggregation through the following mechanism: moist, convective regions correspond to decreased shortwave warming and draw energy from high-energy columns, thus acting as a negative feedback. In contrast to these findings, in a more thorough investigation, Wing and Emanuel (2014) found that shortwave radiation was the dominant force in intermediate stages of aggregation (20-60 days) serving

as a positive feedback, and was a significant positive feedback throughout the evolution of aggregation. This feedback is attributed to the reduced (enhanced) absorption of shortwave radiation in the dry (moist) regions.

5.4.2. LONGWAVE FLUXES. Unlike homogenizing shortwave fluxes, homogenizing longwave fluxes completely inhibited convective aggregation across all domains and resolutions. Thus, longwave cooling is crucial for convective aggregation (Muller and Held, 2012; Bretherton et al., 2005; Arnold and Randall, 2015). According to Wing and Emanuel (2014), the longwave feedback is less straightforward, due to competing effects that result from decreasing moisture in the upper troposphere, and the dominant effect changes throughout the course of the aggregation. In the initial stages of aggregation, the primary longwave effect is due to decreased moisture and thus decreased longwave cooling. The longwave feedback dominates again as the aggregation matures, though this time manifested as a negative feedback. A strong positive longwave feedback in the moist region acts to maintain the convective aggregation primarily due to reduced longwave cooling. Wing and Emanuel (2014) argue that the ability of the longwave feedback to act as either a positive or negative feedback may explain the SST-dependence of convective aggregation, since the SST can cause the longwave to either encourage or inhibit stability.

To investigate the radiative effects between low and high clouds, Arnold and Randall (2015) ran two simulations in which either cloud liquid or cloud ice content were set to zero in radiative calculations, effectively removing the radiative effects of high clouds (cloud ice) and low clouds (cloud water). Findings from this simple switch suggest that low clouds have little effect on the ability of convection to aggregate, whereas the high clouds (and their radiative effects) are largely responsible for the longwave anomalies required for humidity

variability and convective aggregation. Muller and Held (2012), however, found that low cloud radiative cooling was necessary for the onset of convective aggregation.

Not only do longwave fluxes play a role in the development and maintenance of convective radiation, but as discussed in Chapter 2, the longwave cloud effect strongly affects spatial variations of ARC across the globe. In Chapter 7, we look into the effect of clouds on the radiative constraint on the precipitation in the context of convective aggregation.

5.4.3. SURFACE FLUXES. Like interactive longwave fluxes, the inclusion of interactive surface fluxes strongly encourages aggregation, since surface fluxes are largely responsible for the up-gradient transport of MSE, which has been determined to be a major factor in supporting convective aggregation (Muller and Held, 2012; Bretherton et al., 2005). The importance of interactive surface fluxes can be explained by the wind-induced surface heat exchange (WISHE) feedback (Wing and Emanuel, 2014), in which enhanced surface fluxes help to set up and maintain a circulation which, in turn, promotes the fluxes. This acts as a positive feedback, and is comparable in magnitude to the radiative feedbacks.

## 5.5. OBSERVATIONAL EVIDENCE

In response to the growing number of modeling studies on convective aggregation, the following questions arose: (1) Is there any observational evidence of convective aggregation in nature? (2) Can it be quantified? (Tobin et al., 2012). To quantify the degree of aggregation, the CLAUS brightness temperature dataset was analyzed to determine the number of convective clusters, the “clumpiness” of clusters, and a combined metric of the two. Convective aggregation must be measured differently in CRMs, however, because of the



tendency of just a single cluster to exist in the small CRM domain. Therefore, a measure of the bimodality of the moisture distribution in the domain is a useful way to quantify aggregation strength. Their analysis revealed a positive correlation between precipitable water and the density of convective clusters, but a negative correlation between precipitable water and convective aggregation as a whole. A strong negative correlation was found between humidity—strongest in the free troposphere—and the degree of aggregation, due primarily to the dryness of the non-convecting region. Due to competing effects between decreased reflected shortwave radiation and increased OLR, the top-of-atmosphere (TOA) net radiation remained nearly unchanged. This does not imply, however, that the distribution of radiative cooling within the atmosphere remains similarly unaffected. Such a change is likely to cause a response in the large-scale circulation.

These observational findings, showing both the existence and influence of convective aggregation in nature, motivate further investigation of both the causes and effects of convective self-aggregation.

## CHAPTER 6

# MODEL SETUP

### 6.1. SYSTEM FOR ATMOSPHERIC MODELING

The model used in our study was the System for Atmospheric Modeling (SAM) version 6.10.6 (Khairoutdinov and Randall, 2003). SAM is a three-dimensional anelastic model with a doubly periodic domain. Although SAM can be configured as a large-eddy simulation model, we have used it as a cloud-resolving model in order to investigate convective aggregation, as have many others (Bretherton et al., 2005; Khairoutdinov and Emanuel, 2010; Muller and Held, 2012; Wing and Emanuel, 2014). We used the model’s 1-moment and 2-moment (Morrison et al., 2005) microphysics schemes, and interactive radiation with long-wave and shortwave radiative fluxes computed using the RRTM radiation scheme (Mlawer et al., 1997; Clough et al., 2005; Iacono et al., 2008). Radiative fluxes were calculated at each grid column at every timestep (20 s), and data was written every hour.

Following Bretherton et al. (2005), there was no diurnal cycle and the solar constant was set to  $650.83 \text{ W m}^{-2}$  with a zenith angle of  $50.5^\circ$ , resulting in a constant solar insolation of  $413.98 \text{ W m}^{-2}$ . All simulations were run with 64 verticals levels, 3 km resolution, and were initialized with an idealized sounding from the Global Atmospheric Research Program’s Atlantic Field Experiment (GATE) (Houze and Betts, 1981). There was no mean wind, no rotation, and no large-scale forcings other than solar radiation. All simulations were run for a minimum of 100 days to allow sufficient time for aggregation.

## 6.2. SENSITIVITY TESTS

Following Wing and Emanuel (2014), the first simulation was run using a square domain of 768 km, with an SST of 305 K, and 1-moment microphysics. Successive simulations featured the following changes in order to elicit a response in the ARC and precipitation rates:

- Change in microphysics scheme from 1-moment to 2-moment.
- Change in domain size from 768 km to 480 km.
- Change in SST from 305 to 300 K.

In the second part of the study using SAM, the goal shifted to understanding a pulsation of convection that developed in the aggregated state. In addition to the changes mentioned above, evaporation of rain was turned off at all vertical levels in order to prevent the formation of cold pools. In the first set of simulations with no evaporation, the simulations were initialized with previously aggregated conditions; this was to test the persistence of the pulsation. The second set of simulations with no evaporation was initialized with homogeneously moist conditions.

### 6.3. QUANTIFYING AGGREGATION STRENGTH

To measure the degree of aggregation, we calculated the domain-averaged column saturation fraction as a function of time, which removes the temperature dependence inherent in precipitable water (PW) alone, and is a non-dimensional quantity. The column saturation fraction (CSF) is calculated as follows:

$$(6.1) \quad \text{CSF} = \frac{\text{precipitable water (mm)}}{\text{saturated water path (mm)}}$$

Additional metrics of aggregation strength include the skewness of the PW distribution, and the coefficient of variation of the PW.

## CHAPTER 7

# EFFECTS OF CONVECTIVE AGGREGATION ON THE RADIATIVE CONSTRAINT ON PRECIPITATION IN THE SAM

### 7.1. QUANTIFYING AGGREGATION STRENGTH

In order to study the effects of convective aggregation on both the atmospheric energy budget and the hydrologic cycle, it is useful to define a metric that measures the strength of the aggregation. Measuring the degree of convective aggregation in CRMs is not a straightforward task, but there have been various attempts to do so. Looking to the dry region for as indicator of aggregation strength, Jeevanjee and Romps (2013) use the minimum boundary-layer specific humidity to measure aggregation strength, though this method has the disadvantage of not including the wet region as well, so that the bimodality of atmospheric moisture—which is largely what defines convective aggregation—is ignored. Addressing this bimodality, Arnold and Randall (2015) introduce a metric of aggregation intensity that is defined as the difference of the average column saturation fraction in the most humid 20% of columns and the driest 20%. This metric did not work well when applied to our simulations, so we instead use the column saturation fraction, the coefficient of variation, and the skewness of the precipitable water, three non-dimensional quantities which together identify the development of convective aggregation well (Figure 7.1). Together, these plots show that aggregation is characterized by a reduction in average column saturation fraction (due to the drying over the majority of the domain), an increase in the coefficient of variation (due to the increased bimodality of the distribution), and positive skewness (due to a small wet region and large dry region). The advantage of plotting the column saturation fraction as

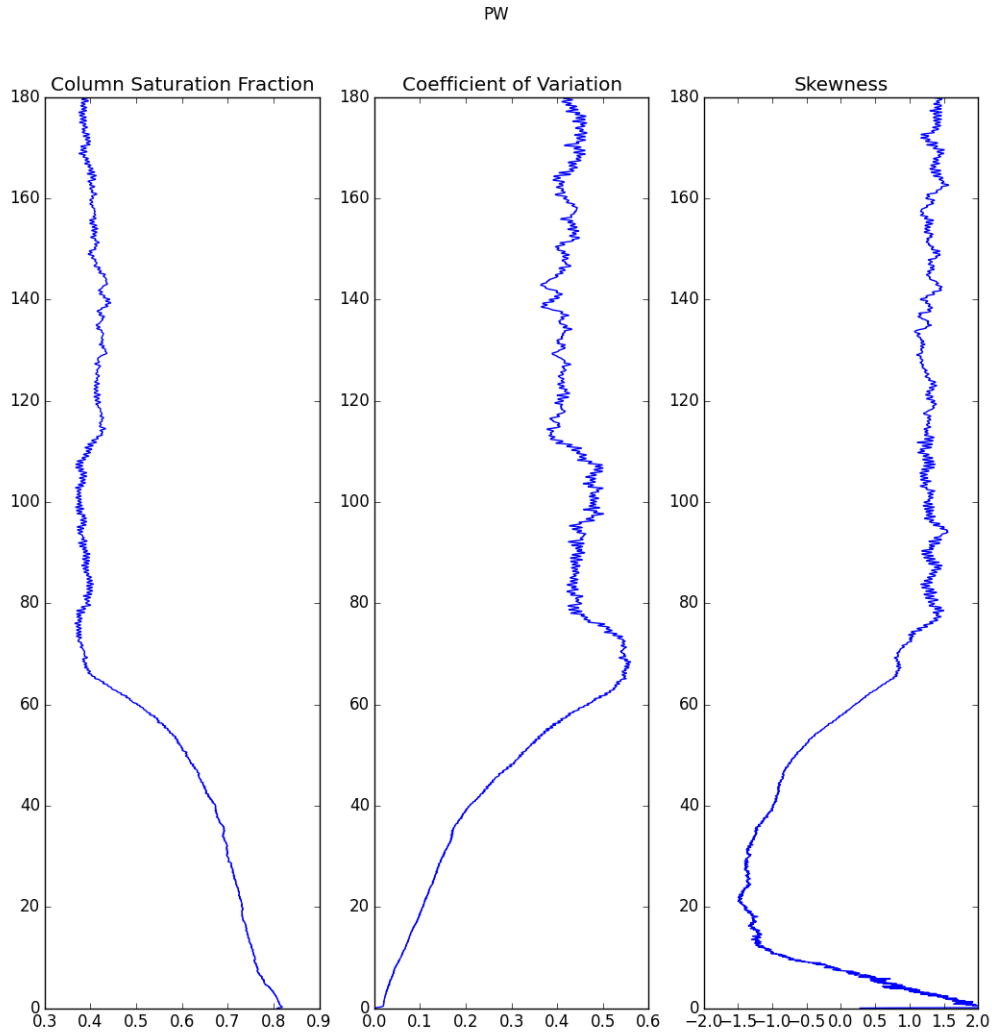


FIGURE 7.1. Suite of statistics on PW distribution that are useful in identifying the evolution and onset of aggregation .

opposed to the mean precipitable water is that the normalization removes the temperature-dependence, and so the saturation fraction can be used to compare aggregation at different SSTs.

To gain a more detailed understanding of the moisture distribution throughout the domain and how it changes as convective aggregation develops, we look at a contour plot of

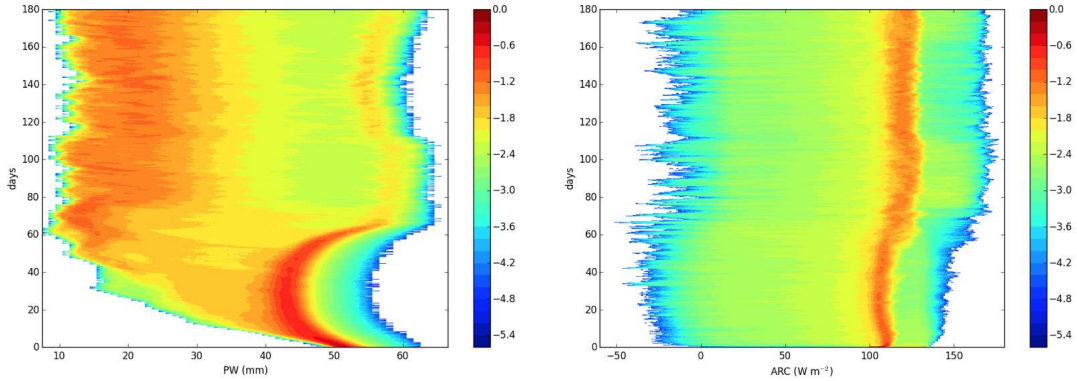


FIGURE 7.2. Contour plot of the PDF of (a) PW (left), and (b) ARC (right), over the domain at each timestep. The color represents the  $(\log_{10})$  fraction of grid points within each bin.

the probability distribution frequency over each day of the simulation. Figure 7.2a shows the percentage ( $\log 10$ ) of grid points with a given amount of precipitable water. The figure shows that the simulation begins with a nearly homogeneous PW distribution of approximately 50 mm, followed by gradual drying over the domain in the first 40 days, and then by 20 days of moistening in some points (the crescent begins to tick right) while others continue to dry. By day 60, the convection has aggregated, with the vertical band of orange on the right-hand side of the figure representing the region of convective activity, while the majority of the domain is characterized by low PW. Near day 100, we see that the average PW of the convective region decreases, showing that although aggregation persists (apparently indefinitely), the degree of aggregation can fluctuate. An analogous plot of the ARC (Figure 7.2b) is visually less interesting than that of PW since the distribution remains generally similar throughout the simulation, but it shows that aggregation is characterized by a shift to higher ARC across the domain.

TABLE 7.1. Overview of the simulations and the name used for reference.

Simulation Name	Microphysics	Domain Size (length)	SST
768HI-1	1-moment	768 km	305 K
768HI-2	2-moment	768 km	305 K
480HI-2	2-moment	480 km	305 K
768LO-2	2-moment	768 km	300 K
480LO-2	2-moment	480 km	300 K

## 7.2. TIME-SERIES ANALYSES: EFFECTS OF CONVECTIVE AGGREGATION

Five different simulations were run using the System for Atmospheric Modeling, sharing the same model setup, except for some differences in microphysics, domain-size, and sea surface temperature (SST); a description of each simulation is given in Table 1. A discussion of the sensitivities to each of these modifications will be given in section 7.3, with the current section focusing on the general trends shared by all simulations. All plots will show the 768LO-2 simulation, which we will refer to as the baseline simulation, unless otherwise noted.

7.2.1. PRECIPITATION. We first look at the time series of the domain-averaged precipitation. Not only is it our primary variable of interest, but it also acts to show the extent of the convective aggregation. Figure 7.3a shows a gradual increase in the precipitation rate, though it is obscured by considerable noise and accompanied by a strong oscillation with a period of approximately 10 hours later in the simulation. In this chapter we will focus solely on the general increasing trend of the precipitation rate, which is more clearly seen by applying a running mean and leave a discussion of this periodicity for Chapter 8. In



Figure 7.4, maps of the daily averaged surface precipitation rate confirm our expectations. Precipitation and other moisture fields start out homogeneously distributed throughout the domain. Precipitation then strengthens as the convection begins to cluster together, and finally maximizes in the aggregated state. The maps in Figure 7.5 nicely show the development of the bimodal moisture distribution beginning with the growth of a single dry patch, also described by Wing and Emanuel (2014). Note that the convection in the baseline simulation first organizes into a band before condensing further into a circle, a pattern observed in all of the simulations with the larger domain size. Wing and Emanuel (2014) observed both banded and circular aggregation patterns as a function of the SST, but no known studies have commented on a domain-size dependence of the evolution of the shape of aggregation.

Because the oscillation can obfuscate the trend in the precipitation (as well as the other variables), a moving average was applied to that data. When viewed using averages over more than 2 days, it is evident that the strongest increase in the precipitation rate occurs in the first 60 days of the simulation, and maximizes at the early stage of aggregation, as the precipitation is clustered into a band (Figure 7.6). These averages reveal a trend hidden in the hourly data: although the precipitation rate remains elevated relative to the pre-aggregation precipitation rate, it does not remain constant. Rather, the precipitation rate decreases weakly and then slowly regains intensity, suggesting that once aggregated, the initial precipitation rate maximum was unsustainable for prolonged periods of time, and was then forced to scale back. It is possible that this change in precipitation strength is tied to a low-frequency fluctuation of domain-averaged moisture, in which the dry region slightly moistens, and thus reduces the strength of the convective aggregation. A slight decrease in

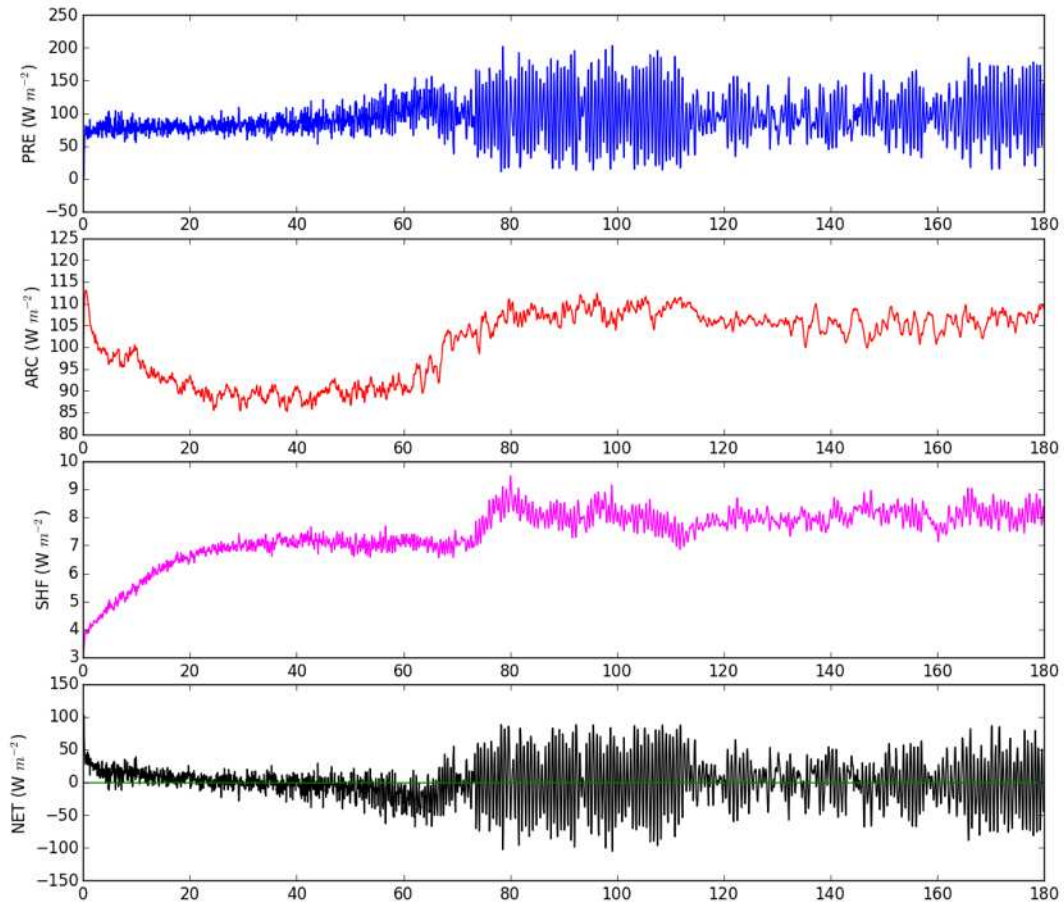


FIGURE 7.3. Domain averages of the fluxes contributing to the atmospheric energy balance. (a) Precipitation (top), (b) ARC (second from top), (c) SHF (second from bottom), (d) Net (bottom).

the aggregation strength can be seen in Figure 7.1 at approximately 115 days, which seems to correspond to the beginning of the drop in the precipitation rate.

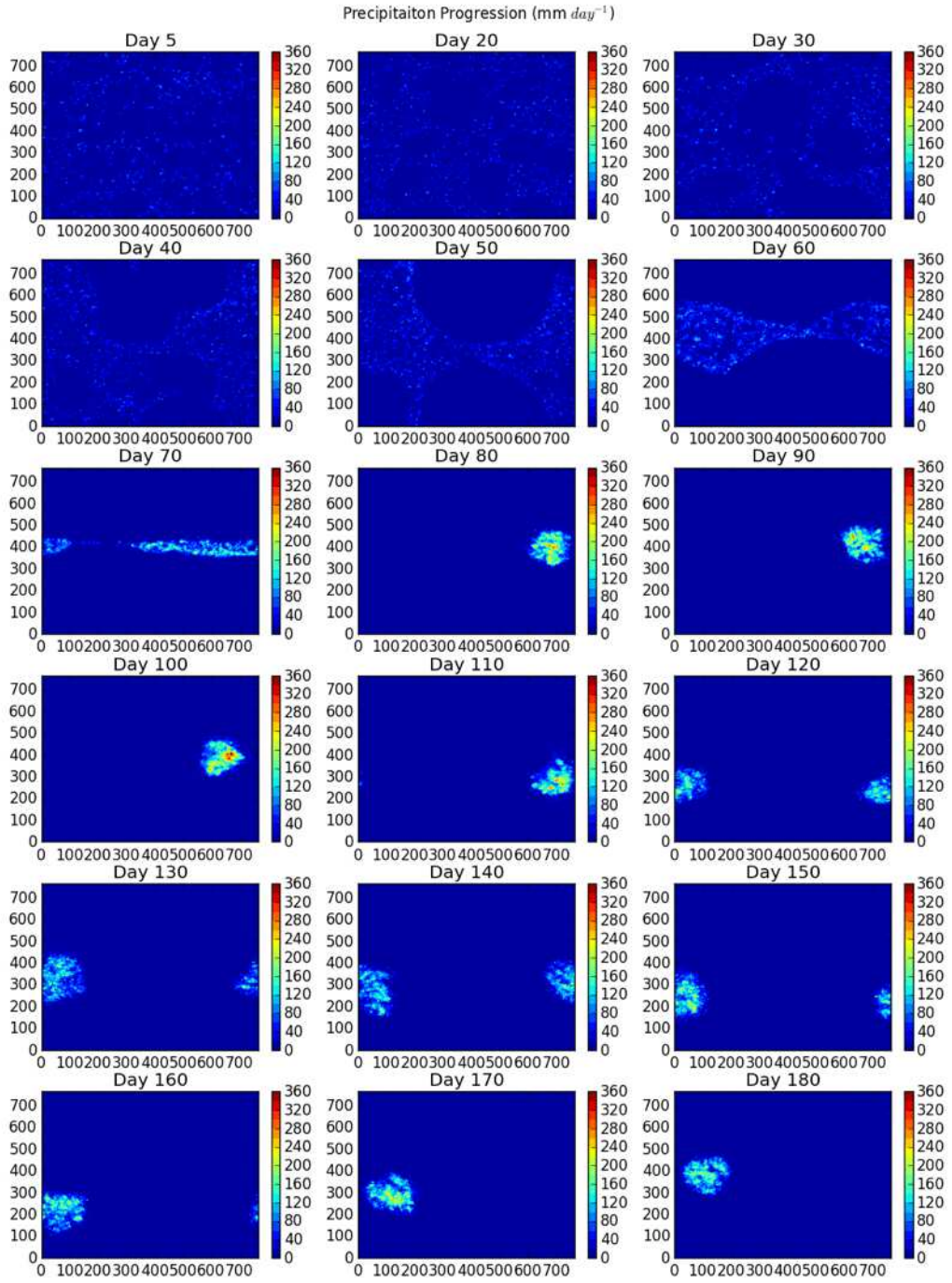


FIGURE 7.4. Maps of the surface precipitation rate averaged over 24 hours.

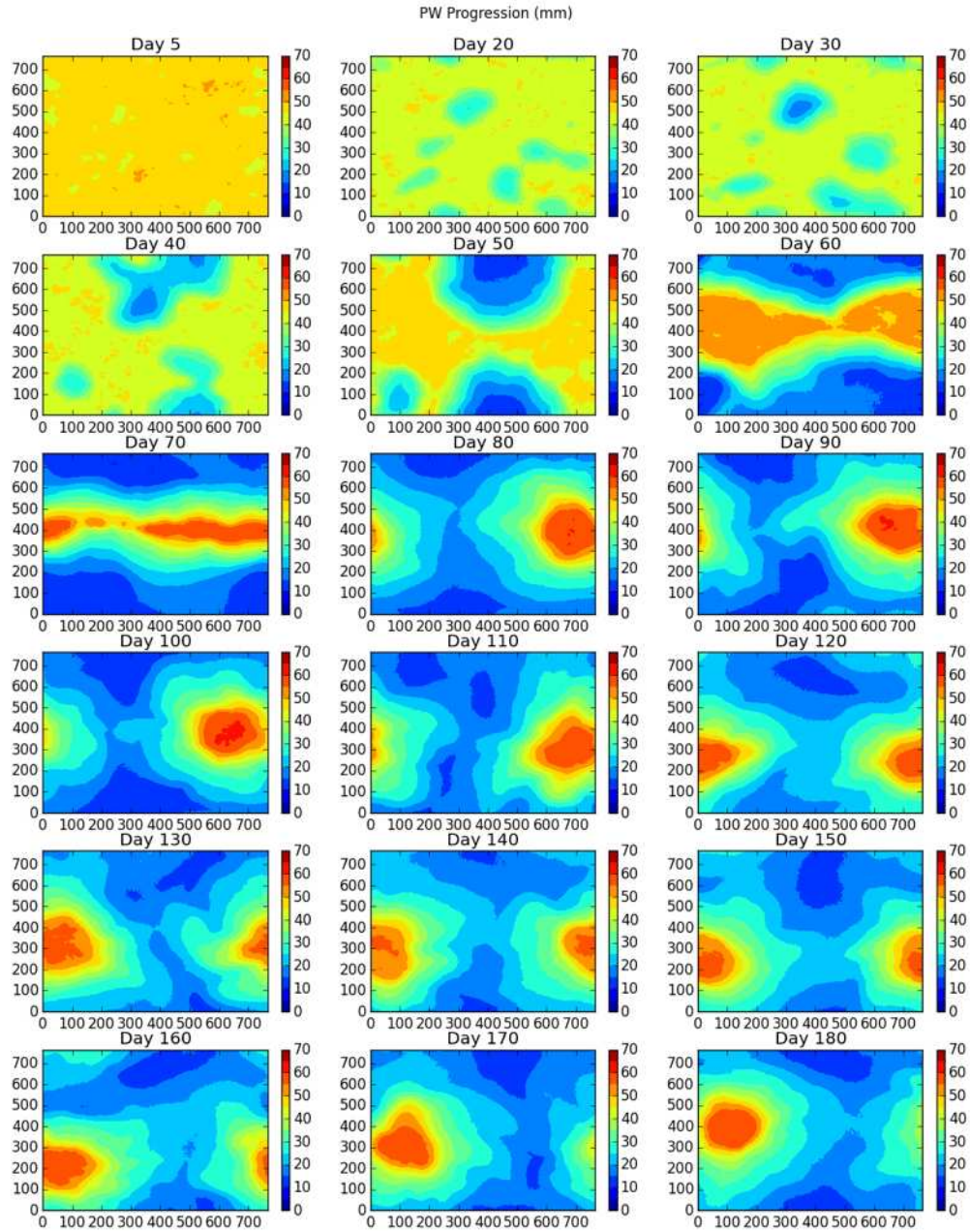


FIGURE 7.5. Maps of PW averaged over 24 hours.

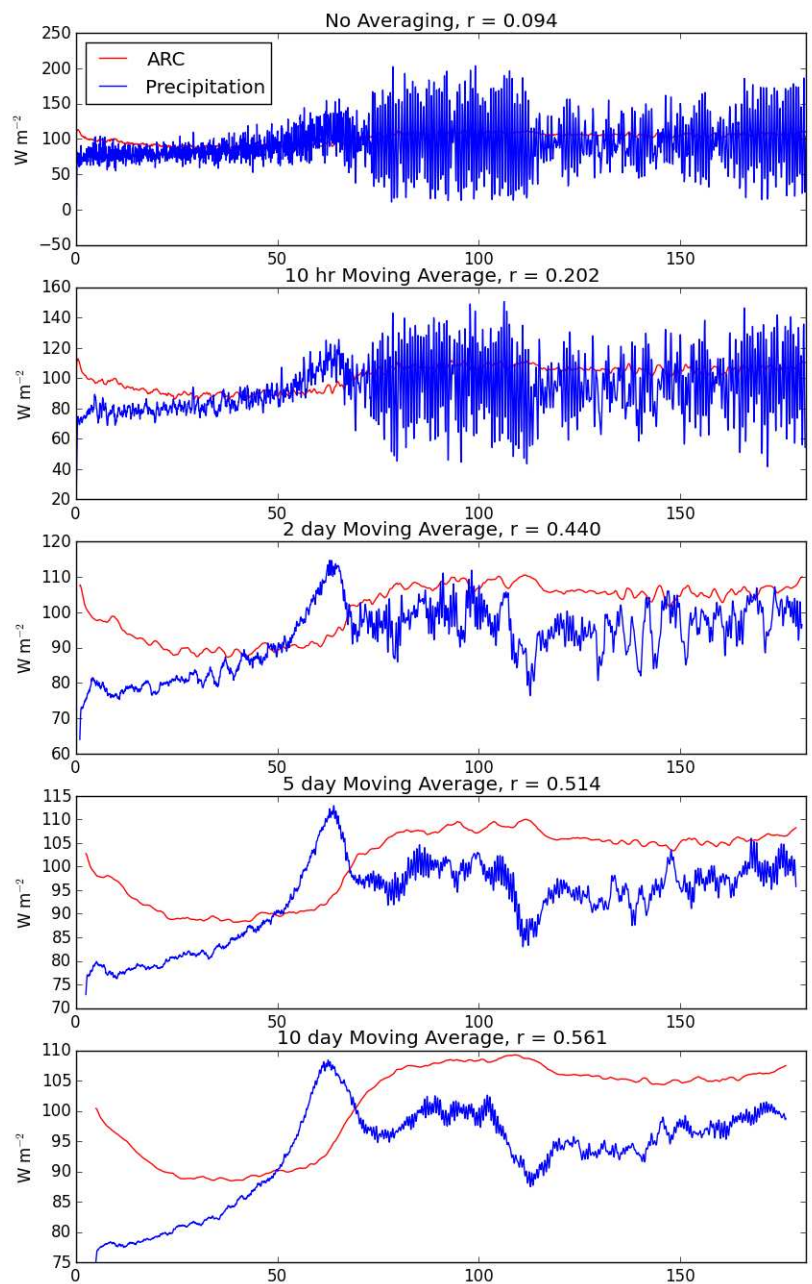


FIGURE 7.6. Running means of the domain-averaged precipitation and ARC.

7.2.2. *ATMOSPHERIC RADIATIVE COOLING.* Like precipitation, the domain-averaged ARC begins low and steadily increases throughout the simulation until equilibrating around day 70 in the baseline simulation. Unlike precipitation, however, the ARC shows no strong oscillation in the convective state (Figure 7.3b). The lack of an oscillation in the ARC can be attributed to the longer persistence of the cloud cover compared to precipitation. Similar to the precipitation rate, however, the moving average shows a similar trend of depressed ARC after convective aggregation has been reached, though the change is not as strong as in the precipitation rate (Figure 7.6).

Comparing the maps of precipitation (Figure 7.4) and the ARC, (Figure 7.7), we see that the regions of high (low) ARC do not perfectly align with regions of low (high) precipitation. This can be explained by the presence of non-precipitating clouds, which, as shown in observations in Chapter 3, can strongly affect the ARC. The strong precipitation observed in the simulation, however, is tied to deep convective clouds alone. This serves as a reminder that the radiative constraints on precipitation act on a broader scale than the precipitation itself.

7.2.3. *OUTGOING LONGWAVE RADIATIVE AND PRECIPITABLE WATER.* The OLR is another variable that is commonly used to detect convective aggregation (Wing and Emanuel, 2014). In Figure 7.8, maps of the OLR show the evolution into a bimodal moisture distribution exhibiting an extremely dry domain with high OLR and a single moist patch with low OLR, aligning well with the structure of the precipitation field. These maps largely appear as a mirror of the ARC maps. As expected, due to the inherent relationship between water vapor and OLR, the same patterns can be seen in maps of the precipitable water (PW), though the PW plots show much smoother contours (Figure 7.5).

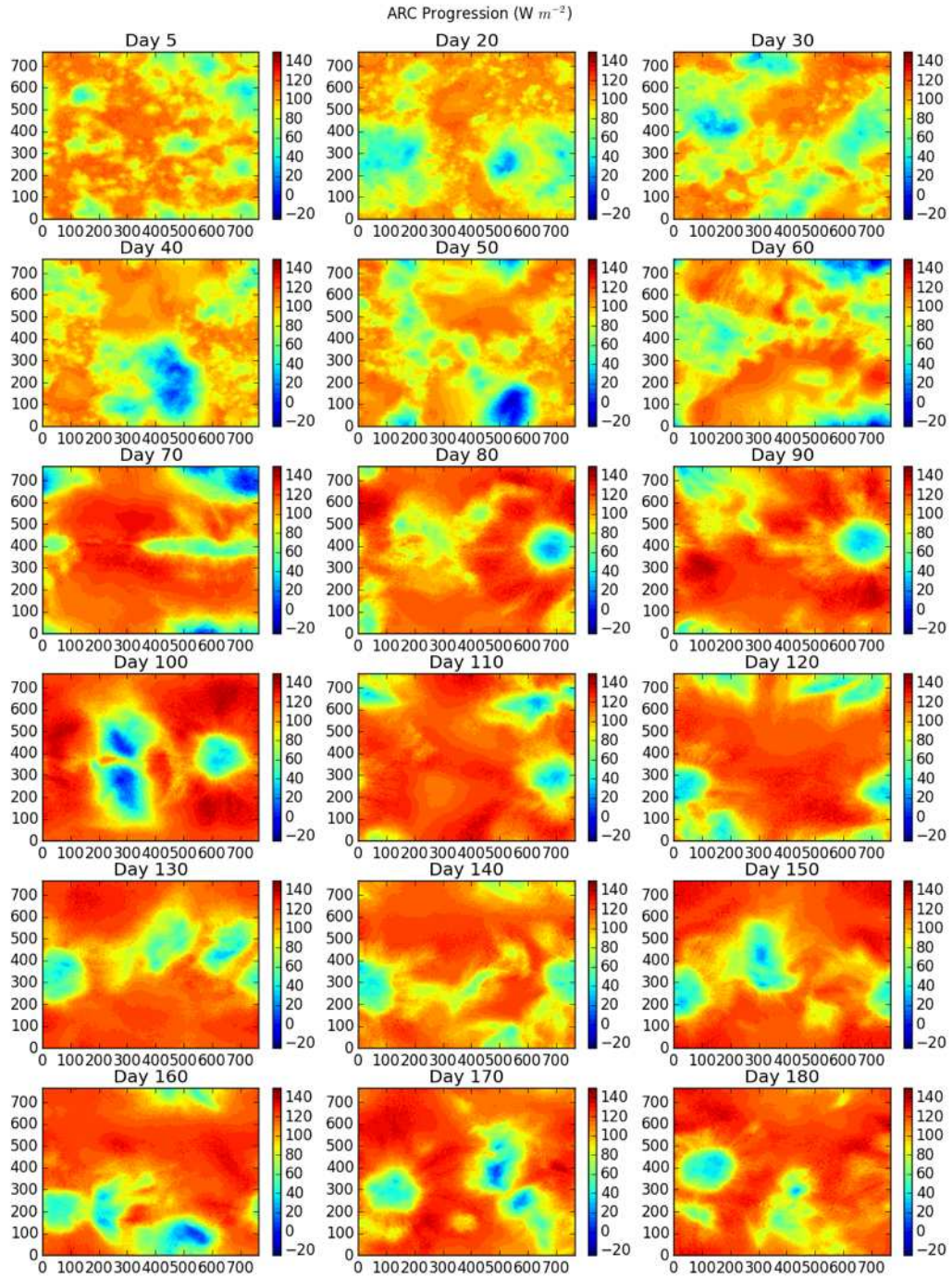


FIGURE 7.7. Maps of ARC averaged over 24 hours.

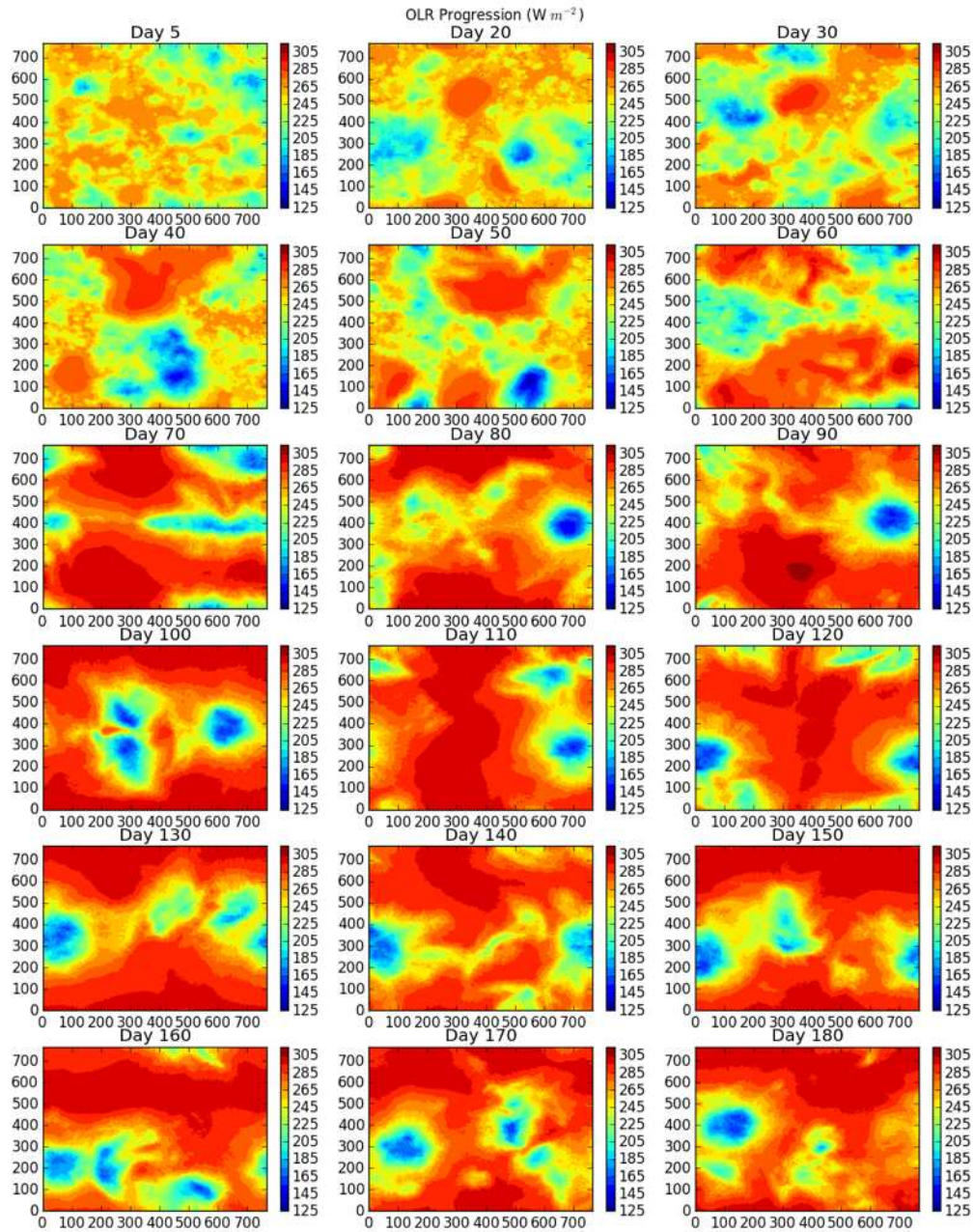


FIGURE 7.8. Maps of OLR averaged over 24 hours.



### 7.3. SENSITIVITY TESTING

We performed sensitivity experiments (Table 1) to modify the model in ways that would affect the ARC, as opposed to directly fixing the ARC as Muller et al. (2011) did. The sensitivity experiments allow us to see the response of the precipitation to changes in the ARC. The runs were identical except for changes to the domain size, SST, and microphysics. The first simulation was run with a warm SST of 305 K in a relatively large 768 km  $\times$  768 km square domain with single-moment microphysics, closely following the experimental design of Wing and Emanuel (2014). The second series of simulations used two-moment microphysics with an SST of 305 K and square domains of two different widths: 480 and 768 km. The third series was identical to the second, but with an SST of 300 K. Although a SST of 300 K falls on the higher end of the spectrum of observed SSTs (and SSTs of 305 K are quite rare in the current climate), our intention was to replicate the results of Wing and Emanuel (2014) and produce an example of strong convective aggregation.

**7.3.1. DOMAIN SIZE.** The second modification was to change the square domain size from a width of 768 km to a smaller domain, though one that would still allow convection to aggregate; a domain width of 480 km was chosen. The results show that decreasing the domain size causes a significant delay in the time of aggregation, which was not completely unexpected (Figure 7.9). Previous studies have found that smaller domain sizes can either prevent aggregation completely (Muller and Held, 2012) or limit the degree of aggregation (Jeevanjee and Romps, 2013).

**7.3.2. SEA SURFACE TEMPERATURE.** Initial simulations were run at 305 K, and then a secondary set was run at a currently more commonly observable SST of 300 K. Both of the simulations at 300 K (768LO-2, 480LO-2) were consistent in producing less ARC

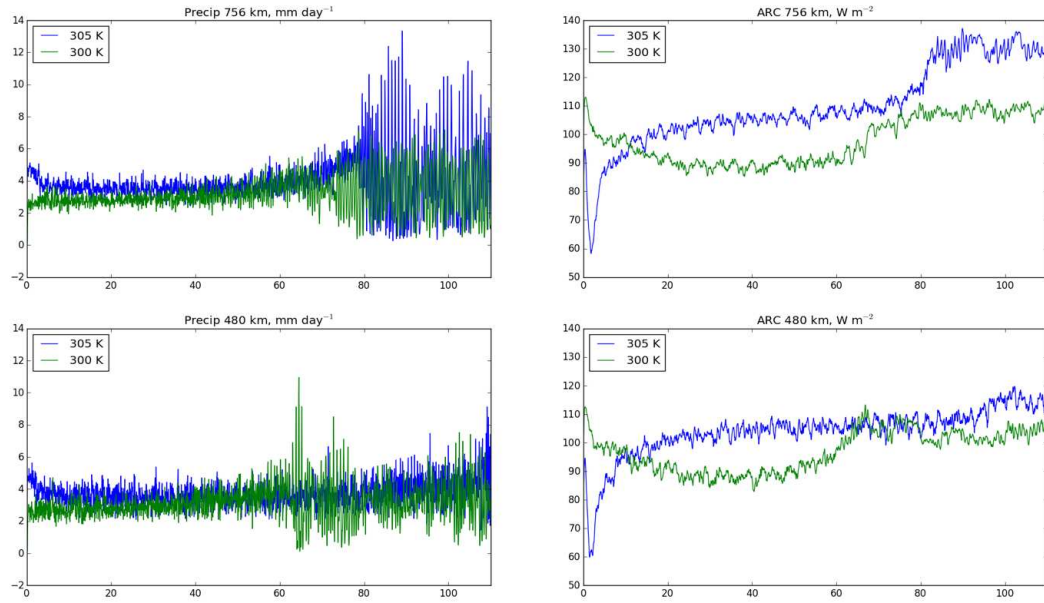


FIGURE 7.9. Comparison of domain-averaged ARC and Precipitation rates at 300 and 305 K , and 480 and 768 km domain.

and precipitation (Figure 7.9). At 305 K, the precipitable water was significantly higher throughout the simulation, and the domain-averaged precipitation rate is stronger. This change could also be attributed to a change in the OLR, which increased with a higher SST, but the change was not as strong. The increase in precipitation with SST agrees with Wing and Emanuel (2014). The difference in precipitation rate for both domain sizes was slightly more than  $0.5 \text{ mm day}^{-1}$ , and persisted over the course of the simulations. These results are consistent with numerous studies suggesting that the hydrologic cycle strengthens in a climate with higher SSTs (Allen and Ingram, 2002; Held and Soden, 2006; Manabe and Wetherald, 1980).

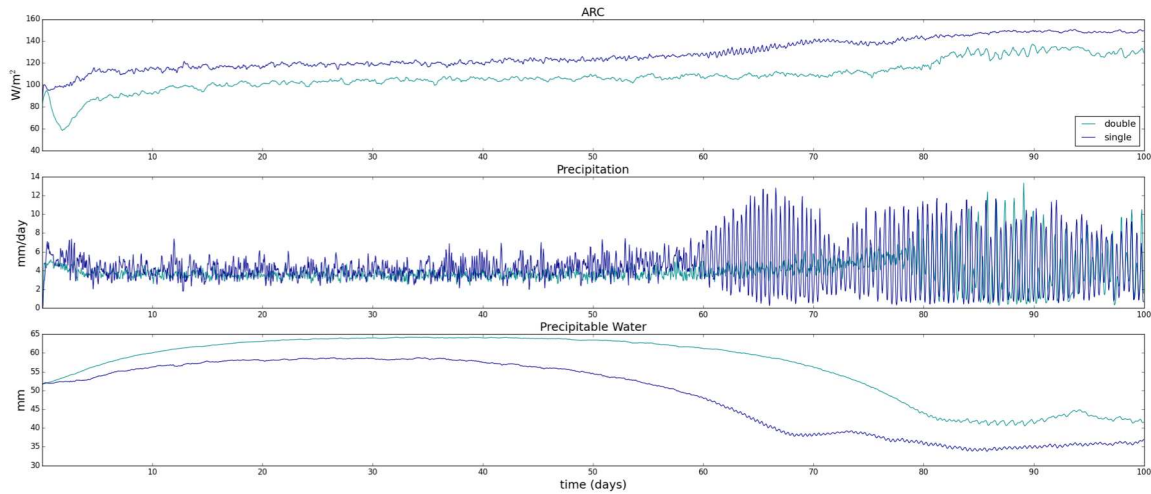


FIGURE 7.10. Comparison of (a) ARC (top), (b) Precipitation (middle), and (c) PW (bottom) with 1-moment and 2-moment microphysics.

7.3.3. MICROPHYSICS. Changing the microphysics was an obvious method to cause a change in the ARC. The majority of studies using SAM to investigate convective aggregation have used only the single-moment microphysics (Bretherton et al., 2005; Wing and Emanuel, 2014), due to the high computational cost of the two-moment microphysics.

Changing to the two-moment microphysics produced two different interesting effects: (1) the time of the aggregation was delayed, and (2), the precipitation rate and ARC both decreased throughout the course of the run (Figure 7.10). An increase in high cloud cover (Figure 7.11) explains this reduction, and could result from a changes in the convective detrainment rate and ice crystal fall speed. An overview of the differences between the 1-moment to 2-moment microphysics parameterizations is given by Morrison et al. (2005).

#### 7.4. TEMPORAL CORRELATION BETWEEN PRECIPITATION AND ARC

As done with the global observations of precipitation and ARC, we calculated the temporal correlation between these fields for each simulation. The data was first averaged over

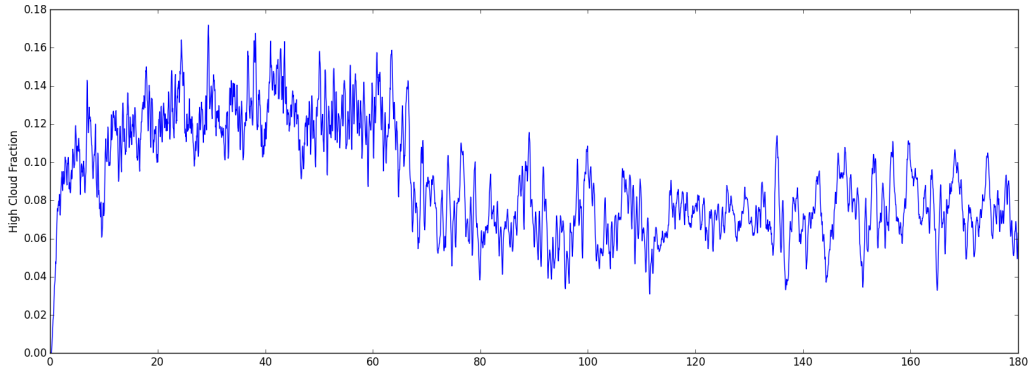


FIGURE 7.11. Domain-averaged high cloud fraction.

a range of time-periods—10 hours, 2 days, 5 days, and 10 days—with the intention of observing how the correlation coefficient changes in response to different averaging times. As expected, the correlation increased with increasing average time (Figure 7.6). In the single-moment simulation, the un-averaged data had a temporal correlation of 0.102, whereas the data averaged over a 30-day period had a correlation of 0.869, mainly reflecting the trends of both variables.

The temporal correlation on a grid point-basis, however, tells a different story altogether. The temporal correlation using the raw data is weakly positive and negative over most of the domain, with a single patch exhibiting an extremely negative correlation corresponding to the convective cluster, and a secondary, though less strong correlation associated with the initial dry patch, as seen in Figure 7.12. The negative correlation is strongly enhanced using the 30-day averaged data. Most of the domain exhibits a very strong negative correlation (-0.8 to -1.0), with a cluster and a separate ring exhibiting a mild positive correlation. Once again, there is a scale-dependence of the correlation between precipitation and ARC. As with the observational results in Chapter 3, although a strong negative correlation can exist between precipitation and ARC on regional scales (most notably in the tropics), the correlation on the global scale must be positive.

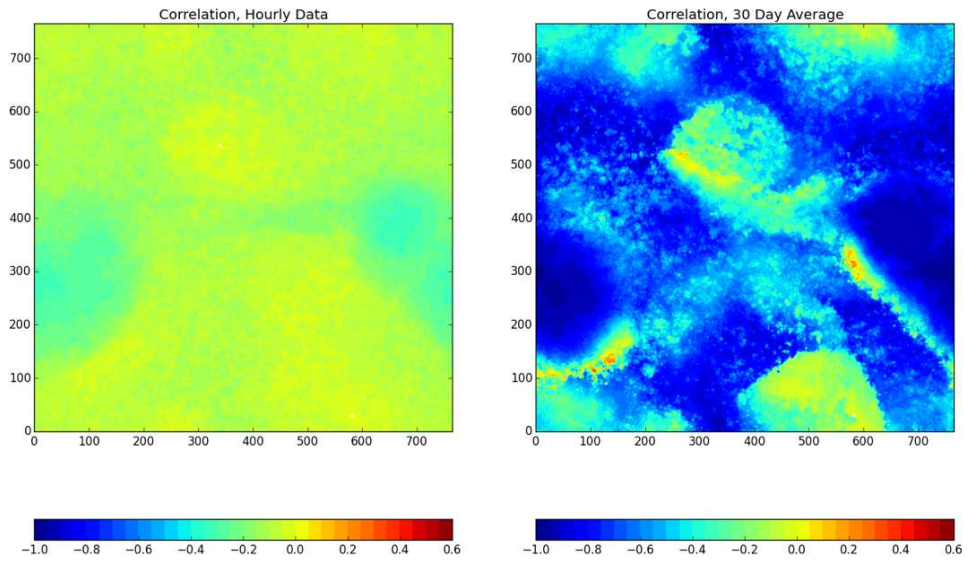


FIGURE 7.12. 2D representation of the temporal correlation between ARC and precipitation at each grid point with (a) no averaging (left) and (b) averaged over 30 days (right).

7.4.1. *ATMOSPHERIC ENERGY BALANCE.* Although not necessarily expected to balance on short time scales, a look at the balance between ARC, the latent heating associated with precipitation, and the surface sensible heat fluxes (SHF) serves as a simple check on the “global” (domain-averaged) energy budget. In this case we consider the following as the net cooling:

$$(7.1) \quad \text{NET} = \text{ARC} - \text{SHF} - \text{LE} \cdot \text{P},$$

where P is the precipitation rate and LE is the latent heat of evaporation. Even with the transient nature of SHF, the net cooling remains close to zero quite consistently, except at the beginning of the simulation as the model spins up, and except for the strong fluctuations in the precipitation rate due to the oscillation (Figure 7.13).

We can gain further insight into the atmospheric energy balance by looking at how the atmospheric heating (latent heating and sensible heat flux) changes over the simulation in relation to the ARC. Figure 7.14 plots the ARC against atmospheric heating (the sum of the latent heat of precipitation and the sensible heat flux); theoretically, if the two quantities were perfectly balance, then the plot showing their changes over the simulation would fall on the line with a slope =1. Looking at the top 2 panels in Figure 7.14, one point sticks out: atmospheric heating is less variable in the beginning of the simulation than at the end, and there is a distinct rise in the ARC after aggregation has occurred (near day 60). Figure 7.14 highlights this jump in the ARC as aggregation occurs. The change in the heating (which is largely dominated by the latent heating of precipitation), however, is not nearly as obvious. Instead, the variability in the aggregated state seems to be the most obvious observation, and the running mean was taken to cover this periodicity. In the 2-day

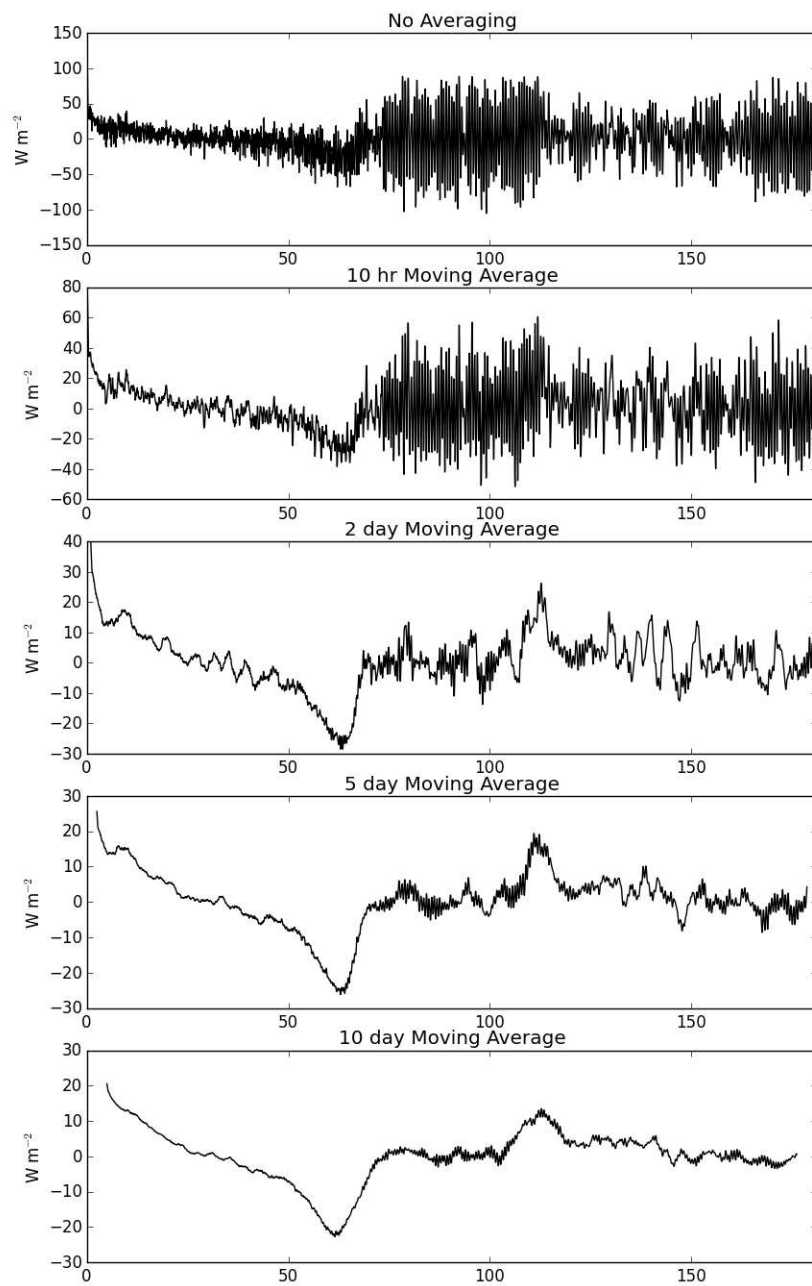


FIGURE 7.13. Running means of the domain-averaged net atmospheric energy balance.

and 10-day running means, the change in the precipitation is more apparent. Precipitation increases as it aggregates—at a much faster rate than the ARC increases—which is followed by a decrease in precipitation as the convection (although aggregated), continues to clump together until its equilibrium aggregated state is reached. During this time, however, the ARC continues to grow. Near the end of the simulation, the heating and cooling approach a balance, with both fields falling on the line representing a one-to-one increase in both ARC and atmospheric heating. The fact that heating and cooling do not align perfectly suggest that there is a lag between the balance of heating and cooling that has not been accounted for. Regardless, the impact of the oscillation on the precipitation rate is highly evident, and in Chapter 8 we look further into both the cause behind its presence and the effect of this periodicity.



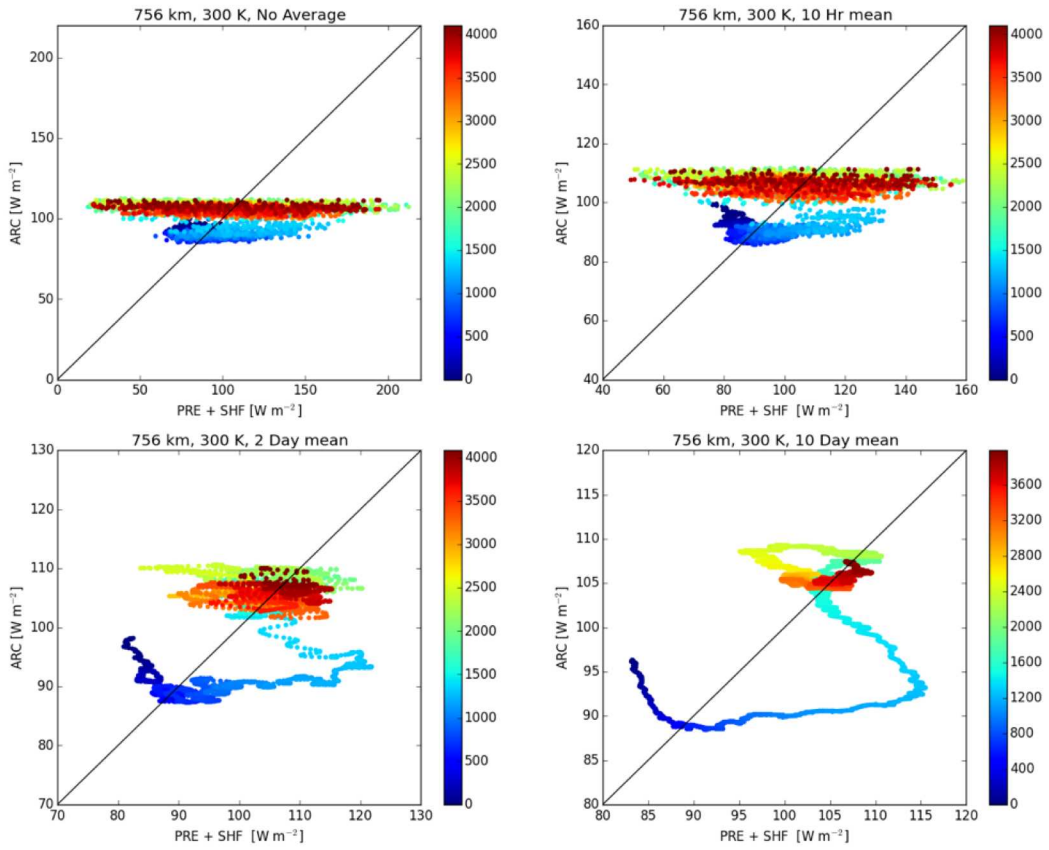


FIGURE 7.14. Changes in ARC plotted against changes in atmospheric heating; running means with various window sizes have been applied. The color indicates the time in hours.

## 7.5. EFFECT OF CLOUDS ON THE ARC

As done in Chapter 3 with observations, we calculated the radiative effect of clouds on the ARC. The clouds act to decrease the ARC in the baseline simulation, as expected for such a warm SST (300 K) (Figure 7.15). When the effect of clouds was calculated for the 768HI-2 simulation, the effect on the ARC was initially stronger than in the baseline simulation, but the cloud effects eventually converged (Figure 7.16). Once convection aggregated, however, the pattern repeated, in which the higher SST initially exhibited a stronger cloud effect, until once again the effect in both simulations converged. Although both simulations show that the effect of clouds is to decrease the ARC, it is surprising that magnitude of the effect varies so little between the two SSTs.

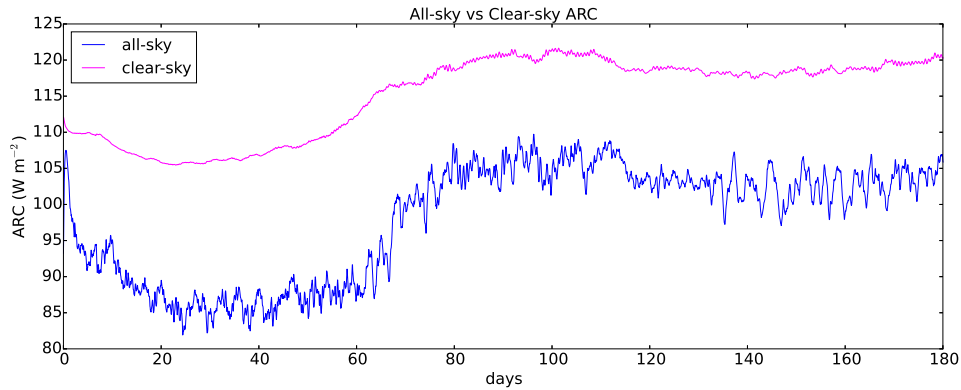


FIGURE 7.15. The cloud effect on the ARC in the baseline simulation.

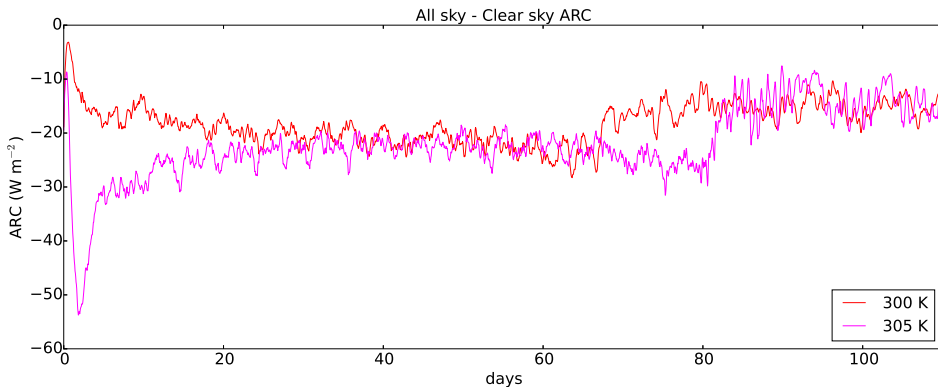


FIGURE 7.16. A comparison of the cloud effects on the ARC in the baseline and 768HI-2 simulations.

## 7.6. CONCLUSIONS

The change from a homogeneous to a bimodal distribution of convection as a result of convective aggregation is evident in plots showing the progression of surface precipitation and PW. Sensitivity tests show that the precipitation rate and ARC are highly sensitive to SST, and both increase with increasing SSTs; this agrees with previous analyses of observational and simulated data (Allen and Ingram, 2002; Held and Soden, 2006; Manabe and Wetherald, 1980). There is also a strong dependence on the microphysics, and 1-moment microphysics produce increased precipitation and ARC due to reduced high cloud amounts

in comparison to the 2-moment microphysics scheme. In all simulations, both the domain-averaged ARC and precipitation rates increased due to convective aggregation, resulting in a positive temporal correlation. A positive correlation is expected because the domain-average in SAM is analogous to the global mean in observations. To our surprise, however, the ARC and precipitation do not necessarily increase at the same times or at the same rates.

We find that at both temperatures of 300 and 305 K, the radiative effect of clouds is to decrease the ARC. This finding is consistent with our results in Chapter 3 and supports our hypothesis, that convective aggregation occurs where the effect of clouds is to decrease the ARC. The extent to which the SST affects the radiative cloud effect on the ARC is not fully clear.

## CHAPTER 8

# PULSATION OF AGGREGATED CONVECTION IN SAM

This chapter is a departure from the previous results chapters; rather than focusing on the relationship between ARC and precipitation, it investigates a pulsation in the convective precipitation simulated by SAM.

### 8.1. OVERVIEW OF THE PHENOMENON

As seen in the previous chapter, a timeseries of the domain-averaged precipitation rate shows the expected amount of noise throughout the entire simulation; this is eventually followed, however, by an unexpected strong oscillation around a base rate that persists throughout the remainder of the simulation. Visualization of the two-dimensional field more accurately shows that the precipitation is in fact pulsing on and off, once aggregation has occurred (Figure 8.1). The pulsation can be observed in other moisture fields (e.g. precipitable water) to a much lesser degree, but is not seen in OLR or ARC, perhaps due to the persistence of clouds in relation to the period of the pulsation. A pulsation of convection has been observed in previous research, though has not received much notice or attention, and has yet to be thoroughly investigated (Wing, 2014, pp. 59-61; P. Blossey, personal communication, August 6, 2015).

### 8.2. HYPOTHESES

We developed several hypotheses that might explain the existence of the pulsation and account for its period. Because of the regularity of the period observed in both simulations, our first hypothesis is that the oscillation is due to gravity waves excited by and feeding back on the convection. This hypothesis implies the period of the oscillation will increase

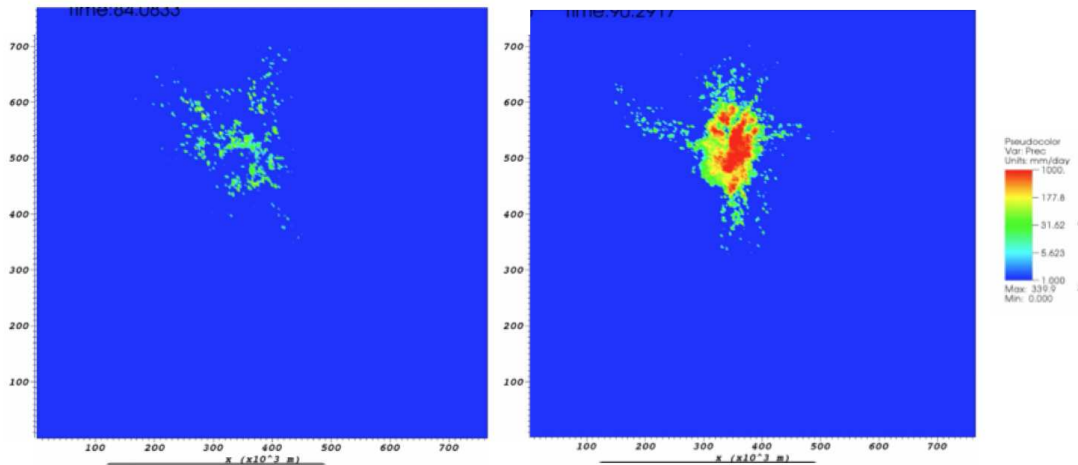


FIGURE 8.1. Snapshot of the surface precipitation pulsing at a relative minimum (left) and maximum (right).

in proportion to the domain size. A second hypothesis, suggested by the signature of the pulsation in the cold pools at the lowest model level (25 m) is that the convective cluster rains out, creating a cold pool at the surface, and effectively shuts itself down. The moist static energy of the boundary-layer air recovers, and it is the recovery time that sets the period of the pulsation. This is analogous to the “discharge-recharge” theory of Bladé and Hartmann (1993), which they proposed in a different context. Our third hypothesis is that both of these processes are occurring in conjunction with each other.

### 8.3. SENSITIVITY TESTING

We used simulations discussed in the previous chapter to test the sensitivity of convective aggregation (and thus ARC and precipitation) to the domain size, SST, and microphysics were used to test the sensitivity of the pulsation to these same parameters. To test for the possible role of cold pools, a further set of experiments was run with the evaporation of falling rain turned off.

8.3.1. DOMAIN SIZE. Reducing the size of the domain—though not so much as to prevent convective aggregation—was an obvious way to test the sensitivity of the period of the oscillation period to domain size. All domains were square, and the width was decreased from 768 km to 480 km. By decreasing the size of the domain but keeping SST constant at 305 K, the period of the oscillation changed from a very steady 10 hours to approximately 7 hours, and later increased to 14 hours (Figure 8.2).

With an SST of 300 K, in the 768LO-1 and 480LO-2 simulations, the effect of changing the domain size was less clear, possibly due to the fact that aggregation was already somewhat hindered by the lower SST. At 768 km, spectral analysis (over the data after aggregation occurred) shows a very clear peak at 10 hours, in agreement with the 768HI-2 simulation. The increased power shown in the power spectra can be attributed to the increased simulation duration (of 180 days) in the 300 K simulations, in which a larger portion of the simulation was spent in the aggregated state. In the 480LO-2, the period of the pulsation becomes ill-defined; instead of a single peak (or even two peaks), a series of peaks in the power spectra presents itself. The lack of clarity observed in the period could be due to the reduced ability of convection to aggregate in the first place, with the combination of both the reduced domain size and lowered SST.

8.3.2. SEA SURFACE TEMPERATURE. Spectral analysis of the simulations at 305 K shows either two distinct peaks (480HI-2) or “packets” of peaks (768HI-2) of the pulsation frequency (Figure 3a,b). Although the two sets of peaks may arise from different reasons, they are certainly well defined. The two sets of peaks in the 480HI-2 simulation represent periods of approximately 7 and 13 hours, and can be traced back to the near-doubling of the period in the last 10 days of the simulation. In the 768HI-2 simulation, the two sets of

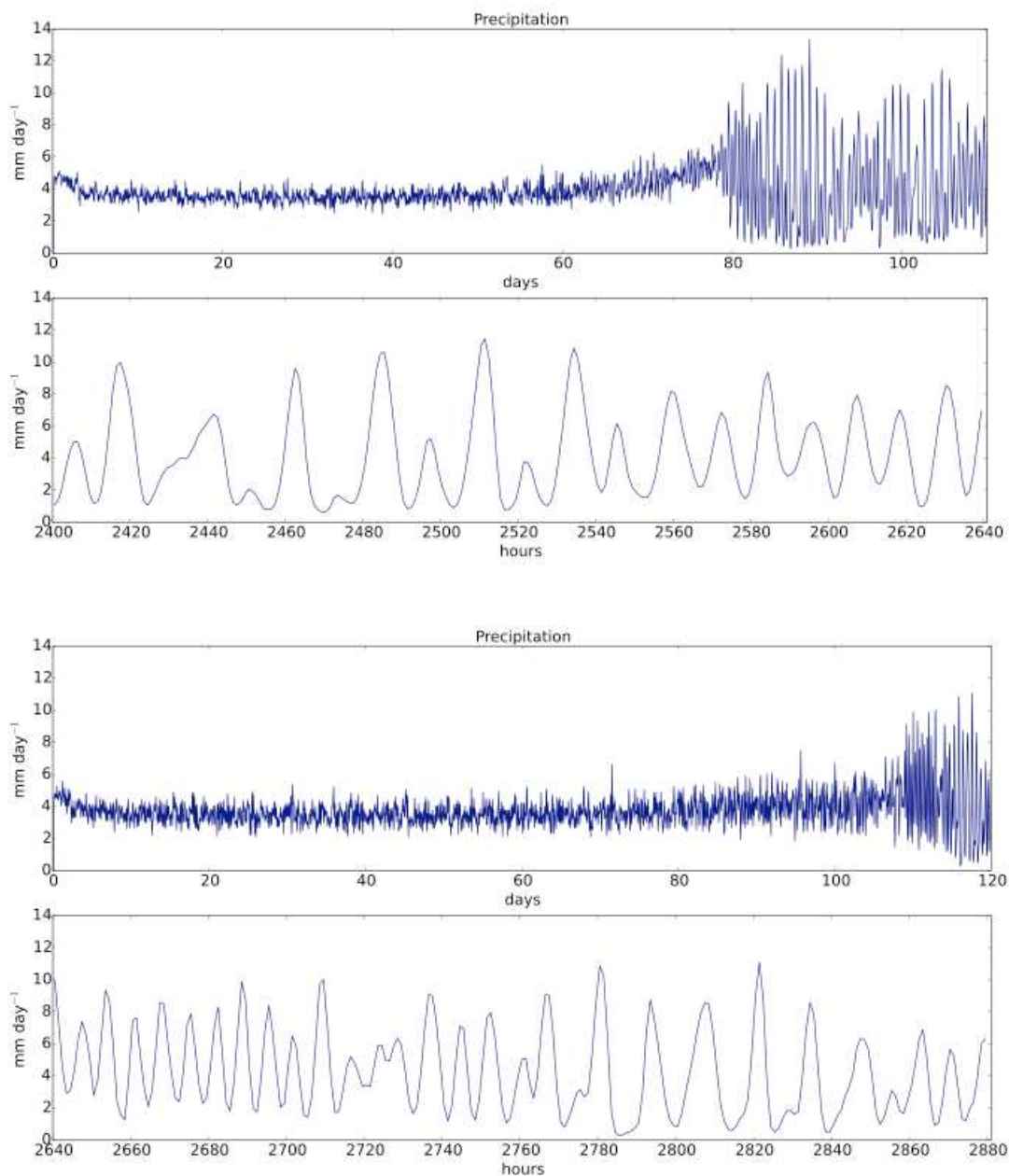


FIGURE 8.2. Top two panels are of 768HI-2 (a) over the entire simulation and (b) with a close up of the final 10 days. Bottom panels (c,d) are the same, but for 480HI-2.

peaks correspond with the two-step oscillation, with a primary period of approximately 10 hours and secondary period (between higher crests and lower crests) of approximately 20



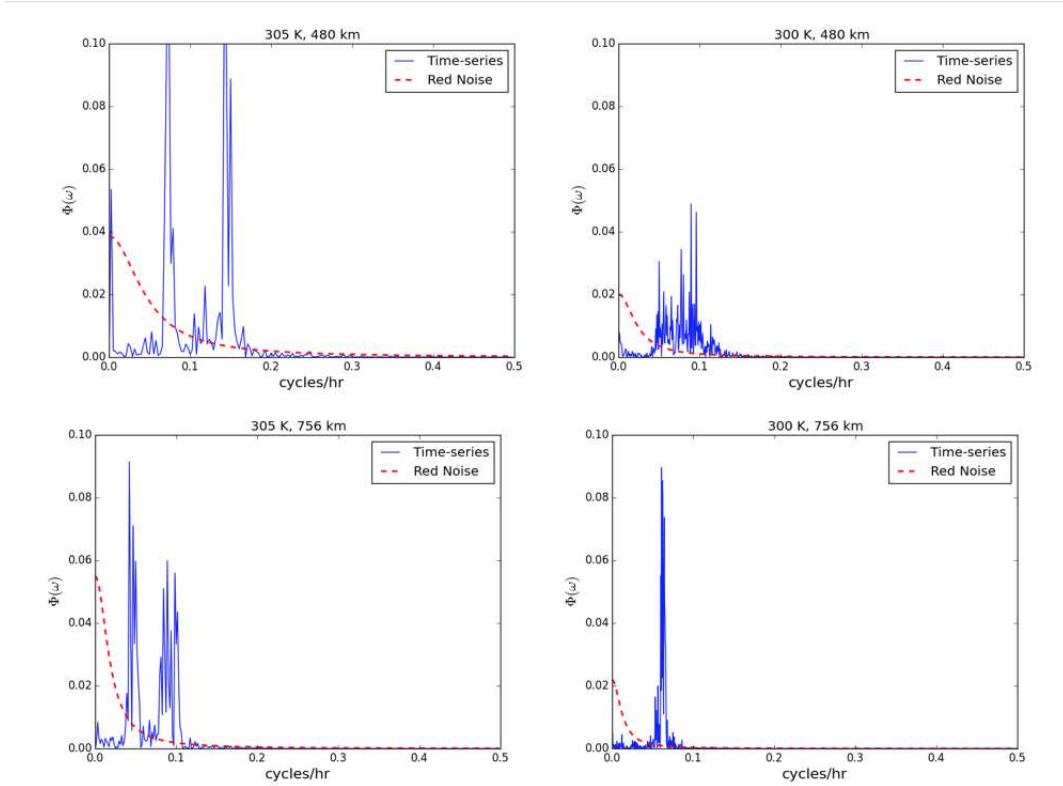


FIGURE 8.3. Spectral analysis of (a) 480HI-2 (top left), (b) 768HI-2 (bottom left), (c) 480LO-2 (top right), (d) 768LO-2 (bottom right)

hours. This pattern is not observed at the lower SST, and spectral analysis of the simulations at 300 K shows no such distinct separation. Whereas the 480LO-2 simulation shows a cluster of peaks ranging from approximately 10 to 24 hours, the 768LO-2 simulation shows a single, though very strong, peak at 10 hours (Figure 8.3c,d). The strength of the signal in the 768LO-2 simulation is a result of the long duration of this simulation, meaning that the aggregated state (and therefore its periodicity) is represented in a larger fraction of the timeseries.

8.3.3. MICROPHYSICS. Originally running the 768HI-1 simulation, the first evidence of the oscillation was found in the domain-averaged precipitation rate, with a period of near 10 hours. A pulsation with a similar period (10.9 hours) was found in the same size domain in Wing (2014). Considering that the oscillation could be due to deficiencies of the

simple microphysics parameterization, and that improved microphysics might eliminate the oscillation, a simulation was performed using 2-moment microphysics. The period was the same in both simulations, though a pronounced two-step oscillation was observed with the two-moment microphysics, in 768HI-2 (Figure 8.2b). In this simulation, the more dominant oscillation appeared to have roughly double the period of the 768HI-1 simulation, with the period remaining the same between peaks of higher and lower amplitudes.

8.3.4. EVAPORATION OF FALLING RAIN. To test whether the pulsation was a result of cold pool formation (and subsequent effect on shutting down convection), several simulations were run in which the evaporation of falling rain was turned off. This is expected to prevent the formation of cold pools. Two tests were run: one with the evaporation turned off in the middle of the run—after the aggregated state had been reached—and the second, in which evaporation was turned off from the beginning of the simulation.

After 120 days (once the aggregated state had been reached and maintained), the 768LO-2 and 480LO-2 simulations were both run, using the end of the original runs as initial conditions, for a sufficiently long time period—in this case 150 days—with evaporation turned off. Supporting our ‘cold pool hypothesis’, once the evaporation was turned off, the pulsation disappeared, though the convection remained aggregated (Figure 8.4). Furthermore, turning evaporation off resulted in increased precipitation, OLR, and ARC, all of which remained elevated throughout the duration of the simulation. We can explain these findings due to reduced detrainment that results from no evaporation. With reduced detrainment, more condensate is available to precipitate out of the cloud, increasing the surface precipitation rate, and therefore, less condensate is available to form high cloud. These changes go hand-in-hand with a decrease in the mid-level and high cloud fractions.

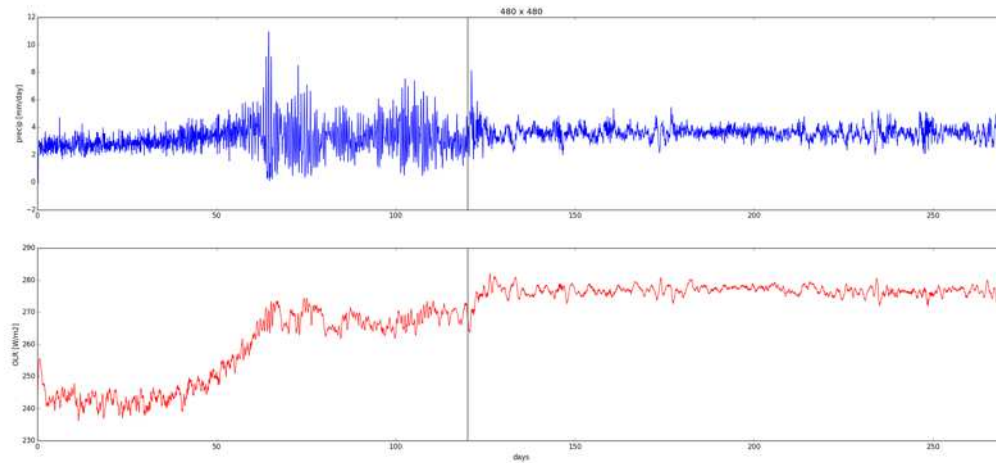


FIGURE 8.4. Domain-averaged (a) precipitation (top) and (b) OLR (bottom) in the 480LO-2 simulation, under initial condition (left of vertical line) and after evaporation is turned off at 120 days.

In the secondary tests with modified evaporation, evaporation was turned off from beginning the beginning of the simulation, with a 480 km domain length and an SST of 300 K. The convection was still found to aggregate by the end of the 80-day simulation, which agrees with previous findings that when cold pools are removed (via turning off evaporation), aggregation has no domain-size dependence (Jeevanjee and Romps, 2013). Although the convection aggregated and there were strong fluctuations in the precipitation rate, there was no regular pulsation (Figure 8.5).

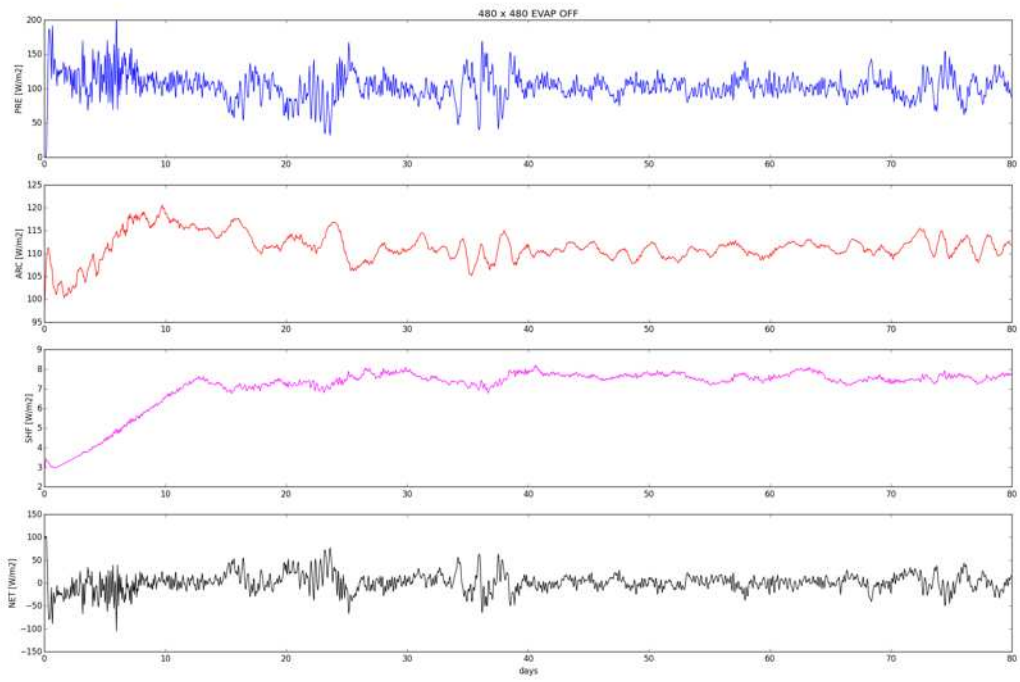


FIGURE 8.5. Domain-averaged (a) precipitation (top), (b) ARC (second from top), (c) SHF (second from bottom), and (d) net cooling (bottom) in the 480LO-2 simulation with evaporation turned off initially.

## 8.4. CONCLUSIONS

Once the convection had aggregated, a pulsation of the convective activity developed. This pulsation was most obvious in the precipitation field, though could be observed to a much smaller degree in other moisture fields, and was obscured in the OLR and ARC due to the persistence of high cloud. The presence of the pulsation is insensitive to domain size, SST, and microphysics. The period of the pulsation, on the other hand, appears to be strongly sensitive to domain size and somewhat sensitive to microphysics (a two-step oscillation developed with the 2-moment microphysics). We can explain sensitivity of the period to domain size by linking it to convection-induced gravity waves; but this does not explain why the pulsation develops in the first place.

After cold pool development and decay was observed to accompany the precipitation pulsation, a new simulation was run with no evaporation of falling rain. This simulation prevented the formation of cold pools, and also prevented the pulsation. The lack of evaporation did not however, inhibit aggregation itself. We speculate that a version of this pulsation could exist in nature, especially over the tropical oceans where both convective clusters and cold pools exist and the diurnal cycle is weak.

## CHAPTER 9

# DISCUSSION AND CONCLUSIONS

### 9.1. OBSERVATIONS

In the first part of this study, we analyzed the observed relationships between the precipitation and ARC. A comparison of the seasonal change in global means reveals that the precipitation rate and the ARC are aligned for half of the year (NH summer), but are strongly out-of-phase during the other half of the year (NH winter). This comparison has two possible explanations: (1) the SHF is weaker during the NH winter than during the NH summer, and (2) there is a time delay on the order of several months in the balance between ARC and precipitation, which is less likely. It would be prudent to investigate a lag in the balance of these two quantities, as well as a hemisphere-dependence of the SHF. The increase of the SHF during the NH summer could possibly be explained by the higher land mass in the NH than in the SH. The interannual variability, much like the seasonal cycle, demonstrates that precipitation and the ARC are not always in phase.

We follow this by looking specifically at the effect of clouds on the ARC. The most apparent observation is that clouds tend to warm the atmosphere (reduce the ARC) in the tropics, and tend to cool (increase the ARC) at higher latitudes. The strong cooling effect is also present where marine stratocumulus decks reside. Together, these observations suggest that high clouds tend to reduce the ARC, and low clouds tend to increase the ARC. We can decompose the ARC into its various components (surface and TOA; longwave and shortwave) to isolate the effects of clouds on each individual component. Doing so, we see that clouds tend to decrease the surface component of the ARC, an effect that is strongest near the equator and acts to increase the surface component of the ARC near the poles,

though this effect is partially compensated for by the influence of clouds increasing the TOA component of the ARC. The dominant effect of clouds, however, is due to the change in longwave radiation. Whereas clouds barely change the shortwave component of the ARC, clouds act to decrease the longwave component of the ARC at low latitudes, and to increase it at higher latitudes, which largely echoes the total effect of clouds: to reduce the ARC at low latitudes, and increase the ARC at high latitudes.

The meridional structure of the temporal correlation of the zonally averaged precipitation and ARC is quite striking: in the tropics, they are strongly negatively correlated on both sides of the equator, but the correlation abruptly becomes positive near 30 N and S. The same general pattern is observed in the zonal average of the temporal correlations (at each grid point), though the poleward change from a negative to positive correlation is far more gradual; this signifies that the correlation at each gridpoint across a given latitude is highly variable, and that that latitude is not the only factor that influences the correlation.

We conclude that the ARC and precipitation are negatively correlated in the tropics because the ARC is reduced there by precipitating cloud systems, and that the ARC and precipitation are positively correlated in higher latitudes because the ARC is increased there by precipitating cloud systems. To the best of our knowledge, this is a new result.

A look at the zonally averaged seasonal cycle of both variables helps to further explain the correlations. Near the equator, a maximum in the precipitation aligns with a minimum in the ARC, and that at high latitudes, the precipitation rate varies little throughout the year, whereas the ARC undergoes major changes throughout the seasonal cycle, resulting in a rather weak correlation.

These observational results motivated us to explore the relationship between precipitation and the ARC in the simplified framework of a cloud-resolving model.

## 9.2. BRIDGE

In addition to our results, contradictory results in other studies pointed to the use of a CRM to investigate the radiative constraint on the hydrologic cycle. Because the change of precipitation in response to warming SSTs is unclear (Huffman et al., 2009; Wentz et al., 2007), coupled with the fact that GCMs tend to produce a very low increase in the precipitation rate compared to the increase in water vapor (Held and Soden, 2006), Mauritsen and Stevens (2015) suggested that GCMs might close this gap by accounting for convective aggregation in convective parameterizations. An effect of convective aggregation is increased precipitation, and so we used convective aggregation in SAM as an opportunity to study how precipitation and the ARC change in this context. Furthermore, we propose that convective aggregation occurs where the effect of clouds is to decrease the ARC, and so we examined the cloud radiative effect on the ARC in our simulations.

## 9.3. EFFECTS OF CONVECTIVE AGGREGATION ON THE ATMOSPHERIC ENERGY BALANCE AND HYDROLOGIC CYCLE IN SAM

We used SAM to simulate convective aggregation in a series of sensitivity tests. We attempted to quantify the degree of convective aggregation through a single metric. The column saturation fraction is a good indicator of aggregation strength, but the coefficient of variation and the skewness of the PW add useful information. A contour plot of the time-dependent PDF of the PW is a useful tool to characterize the changes in the moisture distribution during the aggregation process.

Through a series of sensitivity tests, we were able to produce various changes in the ARC and the precipitation rate. An increase in the SST caused both the domain averaged ARC



and precipitation to increase, as expected, and in agreement with the increase in domain-averaged OLR in Wing and Emanuel (2014). Furthermore, the SST-dependent increase supports Held and Soden (2006), who proposed that the hydrologic cycle will speed up in a warming climate. A more surprising result from the sensitivity tests was the sensitivity to the microphysics, in which the switch from 1-moment to 2-moment microphysics not only delayed the onset of aggregation, but it also caused an increase in the ARC and precipitation rates. Thus far, there have been no other reports on the effect of the microphysics scheme on convective aggregation. The sensitivity that we found may be due to changes in the ice crystal and cloud droplet fall speeds, although further study is needed to confirm this.

When looking at the evolution of aggregation as series of maps plotted over time, it is interesting to see how the aggregation process is reflected in the different variables. In the precipitation rate, the aggregation process is easily observed in the plots showing high contrast between regions of heavy and very light rainfall (or none at all). The same pattern is echoed in the PW, but the decrease in the PW with distance from the convective region throughout the domain is more gradual.

Both the precipitation rate and the ARC increase throughout the aggregation process. The rate of increase, varies, however, and the ARC remains elevated after aggregation has been reached, whereas the precipitation exhibits a slight decrease after the initial increase, though still remaining stronger than before the moisture and convection had aggregated. This becomes more obvious when the oscillation and noise are reduced by applying a moving average to the data. As the window of the moving average increases in width, the correlation between the two quantities increases in strength. We expect the temporal correlation to increase, since the latent heating and the ARC should balance on time scales of a month or

longer. There are, however, departures the net energy balance, which motivates us to look at other factors that might be affecting the energy budget.

Looking at the temporal correlation (30-day running mean) at each grid point as opposed to the domain average, the moist region shows a strong negative correlation between the ARC and precipitation, while the regions where the dry patches first developed generally show varying degrees of a negative correlation. The reason behind the strong negative correlation over the convective region is intuitively clear and is similar to what is seen in observations: since the precipitation has strongly increased and the ARC has strongly decreased, the result is a strong negative correlation. Over the rest of the domain, it is initially surprising that hardly any single point shows a positive correlation, but given that each grid point undergoes such strong changes in moisture (and thus ARC), while the change in precipitation is small in comparison (recall the transition from low precipitation to no precipitation), a large fraction of the domain showing a weak correlation makes sense. In nature it is rare to see such drastic changes, and therefore we do observe a positive correlation over parts of the globe, predominantly at middle and high latitudes.

The radiative effect of clouds is to decrease the ARC at both 300 and 305 K. This finding is consistent with our results in Chapter 3 and supports our hypothesis, that convective aggregation occurs where the effect of clouds is to decrease the ARC, and that convective aggregation is a mode of instability that “switches” on where SSTs are sufficiently warm. Our simulations were only run at high SSTs, and so only support half of our hypothesis; we do not show that aggregation does not occur where the radiative effect of clouds is to increase the ARC. Further, from our simulations of only two SSTs, the extent to which the SST affects the radiative cloud effect on the ARC is not fully clear.

#### 9.4. PULSATING AGGREGATED CONVECTION

While investigating the effects of convective aggregation on the relationship between precipitation and the ARC, a curious and surprising pulsation of convective activity was observed once the simulation had reached a state of convective aggregation. A similar pulsation has been seen in previous work with convective aggregation in SAM, though it has not been widely reported on (Wing, 2014; Peter Blossey, personal communication, August 8, 2015). The presence of the pulsation is not sensitive to changes in SST, domain size, or microphysics, although the period of the pulsation is affected by such modifications. Primarily, the period was proportional to the domain size, and a switch from 1-moment microphysics to 2-moment microphysics appeared to induce a two-step oscillation. Changing the SST did affect the period, but the mechanisms are not fully clear.

The existence of intermittent cold pools that participate in the pulsation suggested that the pulsation was tied to the cold pools, and previous research has shown the significance of cold pools for convective aggregation, particularly in relation to suitable domain sizes (Jeevanjee and Romps, 2013). To test the influence of cold pools on the pulsation, the evaporation of falling rain was turned off at all vertical levels. Although the convection remained aggregated, the pulsation no longer appeared. Not only did preventing the formation of cold pools remove the pulsation, it also acted to increase the precipitation rate and the ARC. Turning off the evaporation of falling rain resulted in a drier atmosphere over the majority of the domain, thus increasing the ARC; it increased the precipitation rate by allowing all falling rain to reach the surface. Although it is obviously not possible to turn off the evaporation of falling rain in the real world, this simulation was useful in isolating the effects of cold pools—which are certainly found in nature—on convective aggregation. It may be

possible to observe similar pulsations over the tropical oceans, although the complications of the real world can easily obscure what is going on.

## 9.5. IMPLICATIONS FOR FUTURE WORK

Although this study has contributed to the investigation of the relationships among clouds, radiation, and precipitation—and how they are affected by convective aggregation—there are many remaining questions. To begin, in the comparison of the globally averaged annual cycle of precipitation and the ARC, why are the two fields out-of-phase for half of the year? This is almost certainly due to changes in the SHF, and further research could look at the seasonal cycles of these three fields to tease out difference between land and ocean, or the northern and southern hemispheres, for example.

In that vein, to what extent does the inclusion of the sensible heat flux in the balance between latent heating and the ARC improve the atmospheric energy balance? Although there is no observed gridded dataset for the SHF, reanalysis data could be used to fill this gap. A similar question could be asked for the energy balance observed in SAM. The fact that the ARC and the precipitation rate increase at different rates throughout the simulation is cause to consider the role of other variables in this balance. In regard to convective aggregation, further work should aim to study the effects of aggregation on the precipitation efficiency. Although we and others have found that precipitation increases in the aggregated state in models, there is some disagreement over this in observations (Tobin et al., 2012). Is the increase due to an increase in the precipitation efficiency in aggregated convective systems, as suggested by Mauritsen and Stevens (2015)?

To further the investigation of our hypothesis that convective aggregation occurs where clouds act to decrease the ARC, and does not occur where clouds act to increase the ARC,

we plan to run additional simulations with SAM, but at lower SSTs. Several studies have found that convective aggregation does not occur below 300 K. By running new simulations with SSTs below 300 K, we can check if convection has aggregated, and whether the radiative effect of clouds increases or decreases the ARC.

Additional questions are specific to the pulsation of the convective aggregation. Although the pulsation was observed in our study as well as other studies that have used SAM, would the pulsation develop in other models? We expect that it would be evident in other CRMs, and we plan to run analogous experiments to those described above, but instead using the Regional Atmospheric Modeling System (Pielke et al., 1992) to test if the pulsation is unique to SAM. Lastly, is there any evidence for this pulsation in the nature? Because of its link to the formation of cold pools, it would be interesting to find evidence of convective clusters raining out and then re-forming in observations, and to explore the effects on the atmospheric energy budget and the hydrologic cycle.

## REFERENCES

- [1] Adler, R. F., and Coauthors, 2003: The version-2 global precipitation climatology project (GPCP) monthly precipitation analysis (1979–present). *Journal of Hydrometeorology*, **4** (6), 1147–1167.
- [2] Allan, R. P., 2006: Variability in clear-sky longwave radiative cooling of the atmosphere. *Journal of Geophysical Research*, **111** (D22).
- [3] Allan, R. P., and B. J. Soden, 2007: Large discrepancy between observed and simulated precipitation trends in the ascending and descending branches of the tropical circulation. *Geophysical Research Letters*, **34** (18).
- [4] Allan, R. P., B. J. Soden, V. O. John, W. Ingram, and P. Good, 2010: Current changes in tropical precipitation. *Environmental Research Letters*, **5** (2), 025 205.
- [5] Allen, M. R., and W. J. Ingram, 2002: Constraints on future changes in climate and the hydrologic cycle. *Nature*, **419** (6903), 224–232.
- [6] Arnold, N. P., and D. A. Randall, 2015: Global-scale convective aggregation: Implications for the madden-julian oscillation. *Journal of Advances in Modeling Earth Systems*, **7** (4), 1499–1518.
- [7] Bladé, I., and D. L. Hartmann, 1993: Tropical intraseasonal oscillations in a simple nonlinear model. *Journal of the atmospheric sciences*, **50** (17), 2922–2939.
- [8] Bretherton, C. S., P. N. Blossey, and M. Khairoutdinov, 2005: An energy-balance analysis of deep convective self-aggregation above uniform sst. *Journal of the Atmospheric Sciences*, **62** (12), 4273–4292.
- [9] Clough, S., M. Shephard, E. Mlawer, J. Delamere, M. Iacono, K. Cady-Pereira, S. Bouk-abara, and P. Brown, 2005: Atmospheric radiative transfer modeling: a summary of the

- aer codes. *Journal of Quantitative Spectroscopy and Radiative Transfer*, **91 (2)**, 233–244.
- [10] Del Genio, A. D., and W. Kovari, 2002: Climatic properties of tropical precipitating convection under varying environmental conditions. *Journal of Climate*, **15 (18)**, 2597–2615.
- [11] Durack, P. J., S. E. Wijffels, and R. J. Matear, 2012: Ocean salinities reveal strong global water cycle intensification during 1950 to 2000. *science*, **336 (6080)**, 455–458.
- [12] Emanuel, K., A. A. Wing, and E. M. Vincent, 2014: Radiative-convective instability. *Journal of Advances in Modeling Earth Systems*, **6 (1)**, 75–90.
- [13] Fu, Q., M. Baker, and D. Hartmann, 2001: Tropical cirrus and water vapor: an effective earth infrared iris feedback? *Atmospheric Chemistry and Physics Discussions*, **1 (1)**, 221–238.
- [14] Hartmann, D. L., and M. L. Michelsen, 2002: No evidence for iris. *Bulletin of the American Meteorological Society*, **83 (2)**, 249.
- [15] Held, I. M., and B. J. Soden, 2006: Robust responses of the hydrological cycle to global warming. *Journal of Climate*, **19 (21)**, 5686–5699.
- [16] Houze, R. A., and A. K. Betts, 1981: Convection in GATE. *Reviews of Geophysics*, **19 (4)**, 541–576.
- [17] Huffman, G. J., R. F. Adler, D. T. Bolvin, and G. Gu, 2009: Improving the global precipitation record: GPCP Version 2.1. *Geophysical Research Letters*, **36 (17)**, 117808.
- [18] Iacono, M. J., J. S. Delamere, E. J. Mlawer, M. W. Shephard, S. A. Clough, and W. D. Collins, 2008: Radiative forcing by long-lived greenhouse gases: Calculations with the AER radiative transfer models. *Journal of Geophysical Research*, **113 (D13)**, d13103.

- [19] Jaeger, L., 1976: *Monatskarten des Niederschlags für die ganze Erde*. Deutscher Wetterdienst.
- [20] Jeevanjee, N., and D. M. Romps, 2013: Convective self-aggregation, cold pools, and domain size. *Geophysical Research Letters*, **40** (5), 994–998.
- [21] Khairoutdinov, M. F., and K. A. Emanuel, 2010: Aggregation of convection and the regulation of tropical climate. Preprints. 29th Conference on Hurricanes and Tropical Meteorology, Tucson, AZ, American Meteorological Society.
- [22] Khairoutdinov, M. F., S. K. Krueger, C.-H. Moeng, P. A. Bogenschutz, and D. A. Randall, 2009: Large-eddy simulation of maritime deep tropical convection. *Journal of Advances in Modeling Earth Systems*, **1** (4), 15.
- [23] Khairoutdinov, M. F., and D. A. Randall, 2003: Cloud resolving modeling of the ARM summer 1997 IOP: Model formulation, results, uncertainties, and sensitivities. *Journal of the Atmospheric Sciences*, **60** (4), 607–625.
- [24] Kilonsky, B. J., and C. Ramage, 1976: A technique for estimating tropical open-ocean rainfall from satellite observations. *Journal of Applied Meteorology*, **15** (9), 972–975.
- [25] Lau, K., and H. Wu, 2011: Climatology and changes in tropical oceanic rainfall characteristics inferred from tropical rainfall measuring mission (TRMM) data (1998–2009). *Journal of Geophysical Research*, **116** (D17).
- [26] Lau, K.-M., and P. H. Chan, 1983: Short-term climate variability and atmospheric teleconnections from satellite-observed outgoing longwave radiation. Part I: Simultaneous relationships. *Journal of the Atmospheric Sciences*, **40** (12), 2735–2750.
- [27] Legates, D. R., and C. J. Willmott, 1990: Mean seasonal and spatial variability in gauge-corrected, global precipitation. *International Journal of Climatology*, **10** (2), 111–127.



- [28] Lilly, D. K., 1968: Models of cloud-topped mixed layers under a strong inversion. *Quarterly Journal of the Royal Meteorological Society*, **94** (401), 292–309.
- [29] Lin, B., B. A. Wielicki, L. H. Chambers, Y. Hu, and K.-M. Xu, 2002: The iris hypothesis: A negative or positive cloud feedback? *Journal of Climate*, **15** (1), 3–7.
- [30] Lindzen, R. S., M.-D. Chou, and A. Y. Hou, 2001: Does the earth have an adaptive infrared iris? *Bulletin of the American Meteorological Society*, **82** (3), 417–432.
- [31] Madden, R. A., and P. R. Julian, 1971: Detection of a 40-50 day oscillation in the zonal wind in the tropical pacific. *Journal of the Atmospheric Sciences*, **28** (5), 702–708.
- [32] Manabe, S., and R. T. Wetherald, 1980: On the distribution of climate change resulting from an increase in CO<sub>2</sub> content of the atmosphere. *Journal of the Atmospheric Sciences*, **37** (1), 99–118.
- [33] Mapes, B., and R. Houze, 1993: Cloud Clusters and Superclusters over the Oceanic Warm Pool. *Monthly Weather Review*, **121**, 1398.
- [34] Mauritsen, T., and B. Stevens, 2015: Missing iris effect as a possible cause of muted hydrological change and high climate sensitivity in models. *Nature Geoscience*, **8** (5), 346–351.
- [35] Mlawer, E. J., S. J. Taubman, P. D. Brown, M. J. Iacono, and S. A. Clough, 1997: Radiative transfer for inhomogeneous atmospheres: RRTM, a validated correlated-k model for the longwave. *Journal of Geophysical Research: Atmospheres*, **102** (D14), 16 663–16 682.
- [36] Morrison, H., J. A. Curry, and V. I. Khvorostyanov, 2005: A new double-moment microphysics parameterization for application in cloud and climate models. Part I: Description. *Journal of the Atmospheric Sciences*, **62** (6), 1665–1677.

- [37] Morrissey, M. L., 1986: A statistical analysis of the relationships among rainfall, outgoing longwave radiation and the moisture budget during January-March 1979. *Monthly Weather Review*, **114** (5), 931–942.
- [38] Motell, C. E., and B. C. Weare, 1987: Estimating tropical pacific rainfall using digital satellite data. *Journal of Climate and Applied Meteorology*, **26** (10), 1436–1446.
- [39] Muller, C., and P. O’Gorman, 2011: An energetic perspective on the regional response of precipitation to climate change. *Nature Climate Change*, **1** (5), 266–271.
- [40] Muller, C. J., and I. M. Held, 2012: Detailed investigation of the self-aggregation of convection in cloud-resolving simulations. *Journal of the Atmospheric Sciences*, **69** (8), 2551–2565.
- [41] O’Gorman, P. A., R. P. Allan, M. P. Byrne, and M. Previdi, 2012: Energetic constraints on precipitation under climate change. *Surveys in Geophysics*, **33** (3-4), 585–608.
- [42] Pendergrass, A. G., and D. L. Hartmann, 2014: The atmospheric energy constraint on global-mean precipitation change. *Journal of Climate*, **27** (2), 757–768.
- [43] Pielke, R. A., and Coauthors, 1992: A comprehensive meteorological modeling system—RAMS. *Meteorology and Atmospheric Physics*, **49** (1-4), 69–91.
- [44] Randall, D., 2012: Atmosphere, clouds, and climate. Princeton University Press.
- [45] Rapp, A. D., C. Kummerow, W. Berg, and B. Griffith, 2005: An evaluation of the proposed mechanism of the adaptive infrared iris hypothesis using TRMM VIRS and PR measurements. *Journal of Climate*, **18** (20), 4185–4194.
- [46] Stephens, G. L., and T. D. Ellis, 2008: Controls of global-mean precipitation increases in global warming gcm experiments. *Journal of Climate*, **21** (23), 6141–6155.

- [47] Tobin, I., S. Bony, C. E. Holloway, J.-Y. Grandpeix, G. Seze, D. Coppin, S. J. Woolnough, and R. Roca, 2013: Does convective aggregation need to be represented in cumulus parameterizations? *Journal of Advances in Modeling Earth Systems*, **5** (4), 692–703.
- [48] Tobin, I., S. Bony, and R. Roca, 2012: Observational evidence for relationships between the degree of aggregation of deep convection, water vapor, surface fluxes, and radiation. *Journal of Climate*, **25** (20), 6885–6904.
- [49] Trenberth, K., and Coauthors, 2007: Observations: surface and atmospheric climate change. *IPCC, Climate Change*, 235–336.
- [50] Vecchi, G. A., and B. J. Soden, 2007: Global warming and the weakening of the tropical circulation. *Journal of Climate*, **20** (17), 4316–4340.
- [51] Wentz, F. J., L. Ricciardulli, K. Hilburn, and C. Mears, 2007: How much more rain will global warming bring? *Science*, **317** (5835), 233–235.
- [52] Wielicki, B. A., B. R. Barkstrom, E. F. Harrison, R. B. Lee III, G. Louis Smith, and J. E. Cooper, 1996: Clouds and the earth’s radiant energy system (CERES): An earth observing system experiment. *Bulletin of the American Meteorological Society*, **77** (5), 853–868.
- [53] Wing, A. A., 2014: Physical mechanisms controlling self-aggregation of convection in idealized numerical modeling simulations. Ph.D. thesis, Massachusetts Institute of Technology.
- [54] Wing, A. A., and K. Emanuel, 2014: Physical mechanisms controlling self-aggregation of convection in idealized numerical modeling simulations. *Journal of Advances in Modeling Earth Systems*, **6**, 59–74.

- [55] Xie, P., and P. A. Arkin, 1998: Global monthly precipitation estimates from satellite-observed outgoing longwave radiation. *Journal of Climate*, **11** (2), 137–164.
- [56] Zhang, C., B. E. Mapes, and B. J. Soden, 2003: Bimodality in tropical water vapour. *Quarterly Journal of the Royal Meteorological Society*, **129** (594), 2847–2866.